Bull. Min. Res. Exp. (2024) 173: 55-83

Bulletin of the Mineral Research and Exploration

http://bulletin.mta.gov.tr

Vitrinite reflectances and mineralogy of coal clasts in the Late Carboniferous sequences in the two-deep research wells from the Kozlu coalfield (Zonguldak Basin, NW Türkiye)

Ali İhsan KARAYİĞİT[a*] and Rıza Görkem OSKAY[b]

[a] *Hacettepe University, Faculty of Engineering, Department of Geological Engineering, Ankara, Türkiye*
[b] *Hacettepe University, Başkent OSB Technical Sciences Vocational School, Ankara, Türkiye*

Research Article

Keywords:
Zonguldak Basin, Late Carboniferous, Coal Petrography, Coal Clast, Erosion of Coal Seams.

Received Date: 16.07.2022
Accepted Date: 23.11.2022

ABSTRACT

Fifty-four coal clast samples in the siliciclastic rocks (e.g., sandstone and conglomerate) were collected from cores of two-deep research wells (K20H and K20K) drilled at the Kozlu coalfield in Zonguldak Basin, and for the first time, they were evaluated using mineralogy by XRD and SEM-EDX and random vitrinite reflectance (%Rr) measurements in order to find out their origin and timing. Petrographic observations on polish surfaces show that the coal clasts are either entirely xylitic/vitrinitic particles or coals including a broader range of macerals. The detected minerals in the samples are mostly derived from the parental coal seams and, to a lesser extent, precipitated from penetrated pore-water in the cleats/fractures of clasts. The %Rr values of coal clasts in Carboniferous sediments are generally relatively higher than those measured in the coal seams due to weak oxidation during transportation. Furthermore, similar mineralogical and maceral compositions between coal clasts and coal seams imply that these clasts were mainly eroded during the peatification and/or early coalification of parental seams and display similar coalification patterns. The close %Rr value of a coal clast sample in the Early Aptian Zonguldak Formation and Carboniferous coal seams could suggest that this coal clast sample is presumably derived from the coal seams eroded during Early Aptian.

1. Introduction

Peat beds and coal-bearing sequences could be eroded due to several reasons (e.g., flooding events and mass movements during peat formation or fluvial and marine influence after coalification) (Petersen et al., 1998; Geršlová et al., 2016; Izart et al., 2016; Martínek et al., 2017; Bicca et al., 2020). As a result, coal clasts and/or coal-placers could be observed within the synchronous siliciclastic sediments and marine carbonates of coal seams and in modern marine sediments (Littke et al., 1989; Hower et al., 2001; Pešek and Sýkorová, 2006; Dill et al., 2017, 2021; Zhang et al., 2019; Yang et al., 2020). Coal clasts are commonly found in Carboniferous coal-bearing sequences and range in size from a millimeter to tens of centimeters. Fragments of pebble-sized coal particles and/or in some cases coalified woody material (xylite) within clastic sediments (e.g., sandstone, conglomerate) were reported from several late Palaeozoic coal basins in Europe since the early 20th century (Pešek and Sýkorová, 2006). However, there are a limited number of detailed studies conducted on coal clasts mainly focused within Late Carboniferous coal basins in central Europe and South

Citation Info: Karayiğit, A. İ. , Oskay, R. G. 2024. Vitrinite reflectances and mineralogy of coal clasts in the Late Carboniferous sequences in the two-deep research wells from the Kozlu coalfield (Zonguldak Basin, NW Türkiye). Bulletin of the Mineral Research and Exploration 173, 55-83. https://doi.org/10.19111/bulletinofmre.1209127

Corresponding author: Ali İhsan KARAYİĞİT, aik@hacettepe.edu.tr

Wales (Littke et al., 1989; Paszkowski et al. 1995; Gayer et al., 1996; Kožušníková et al., 1999; Daněk et al., 2002; Misz-Kennan et al., 2019; Suchý et al., 2019; Yang et al., 2020). These studies show that the maceral and mineralogical composition, random vitrinite reflectance (%Rr) values, palynological properties, and size and shapes could provide data about the timing of erosion of Late Carboniferous seams, the origin and possible transportation distance (e.g., a short distance) of coal clasts, and, in some cases, maturation and coal bed methane potential of late Palaeozoic coal-bearing sequences. For instance, the relatively lower %Rr values of coal clasts than the closest late Palaeozoic coal seams within the basin could imply that coal clasts are derived from coal seams in the proximity of coal-bearing sequence due to erosion of these coal seams before coalification. Furthermore, their palynoflora composition could also provide their origin, and more importantly, whether the coal clast-bearing sediments were deposited after a hiatus.

The Zonguldak Basin is located in the NW Türkiye (Figure 1a) and hosts major economic bituminous coal resources in Türkiye within the late Palaeozoic sequences (Figure 1b and 1c) (Karayiğit et al., 1998; 2018*a*). Previous studies of the coal seams of Carboniferous age in the Zonguldak Basin show that the late Paleozoic coal seams display similar palynoflora and coal petrographical features to late Palaeozoic coal basins in the east and central Europe (Akgün and Akyol, 1992; Karayiğit, 1992; Karayiğit et al., 1998, 2018*a*, *b*; Cleal and Van Waveren, 2012; Cleal et al., 2017, 2018; Opluštil et al., 2018). Furthermore, the sedimentological data from the Carboniferous coal seams show that the roof rocks of Carboniferous coal seams are mainly made up of conglomerates and sandstones, which mostly overlie coal seams with erosional bases, and possible erosion of Early Carboniferous (Serpukhovian-Bashkirian) sequences during the Late Carboniferous (Duckmantian-Asturian) was also assumed (Zijlstra, 1952; Kerey, 1985; Opluštil et al., 2018). In addition, the 1-D thermal history modelling from coal seams in the Zonguldak Basin implies possible erosion events during the Carboniferous, Permian, and afterward (Yalçın et al., 2002; Karayiğit et al., 2018*a*). Hence, it is acceptable to observe coal clasts within Carboniferous and Cretaceous sequences in the Zonguldak Basin, but no data was published regarding the coal clasts from coal mines in the Zonguldak Basin. However, during the late 1990s, several deep research wells were drilled by Turkish Hard Coal Enterprise (TTK) in the Kozlu coalfield in order to find out the evolution, geological features, and coalbed methane potential of coal seams within the Carboniferous formations (Alaacağzı, Kozlu, and Karadon, Formations) (Figures 1c and 1d), and several studies have been done from these exploration wells (e.g., Gürdal and Yalçın, 2000, 2001, Yürüm et al., 2001*a, b*; Yalçın et al., 2002; Gürdal et al., 2004; Karayiğit et al., 2018*a*). During the drilling, several coal clast-bearing sediments were cored from Carboniferous formations (Oktay, 1995); however, only very limited palynological data from coal clasts from the Karadon Formation were conducted for age determination (Akgün et al., 1997) and no petrographical investigation and/or their origins have been reported to date. This study aims to present the first detailed vitrinite reflectance and mineralogical data of Late Palaeozoic, as well as Early Aptian coal clast within İnciğez clastics in the Zonguldak Basin. The special target of the study is to find out the origin and timing of these coal clasts in order to estimate whether the erosion took place during peat accumulation or coal formation.

2. Geological Settings

The pre-Carboniferous basement rocks in the basin are mainly the Silurian Hamzafakı Formation (metasediments and shales with diabase and andesite dykes and sills) and the Devonian Göktepe (metasediments with diabase and andesite dykes) and Yılanlı (marine limestone and dolomite) formations (Figure 1b). The Carboniferous coal-bearing sequences are divided into three formations, namely, Alacaağzı, Kozlu, and Karadon (Figure 1b). The Alacaağzı Formation is composed of alterations of sandstone, claystone, siltstone, and coal seams (Figure 1b), which were deposited under deltaic conditions during Serpukhovian-Bashkirian (Namurian) (Ağralı, 1963; Akyol, 1972, Kerey, 1985; Akgün and Akyol, 1992; Yalçın et al., 2002; Cleal et al., 2017). The Kozlu Formation conformably overlays the Alacaağzı Formation and consists of conglomerate, sandstone, siltstone, claystone, and coal seams alternations (Figure

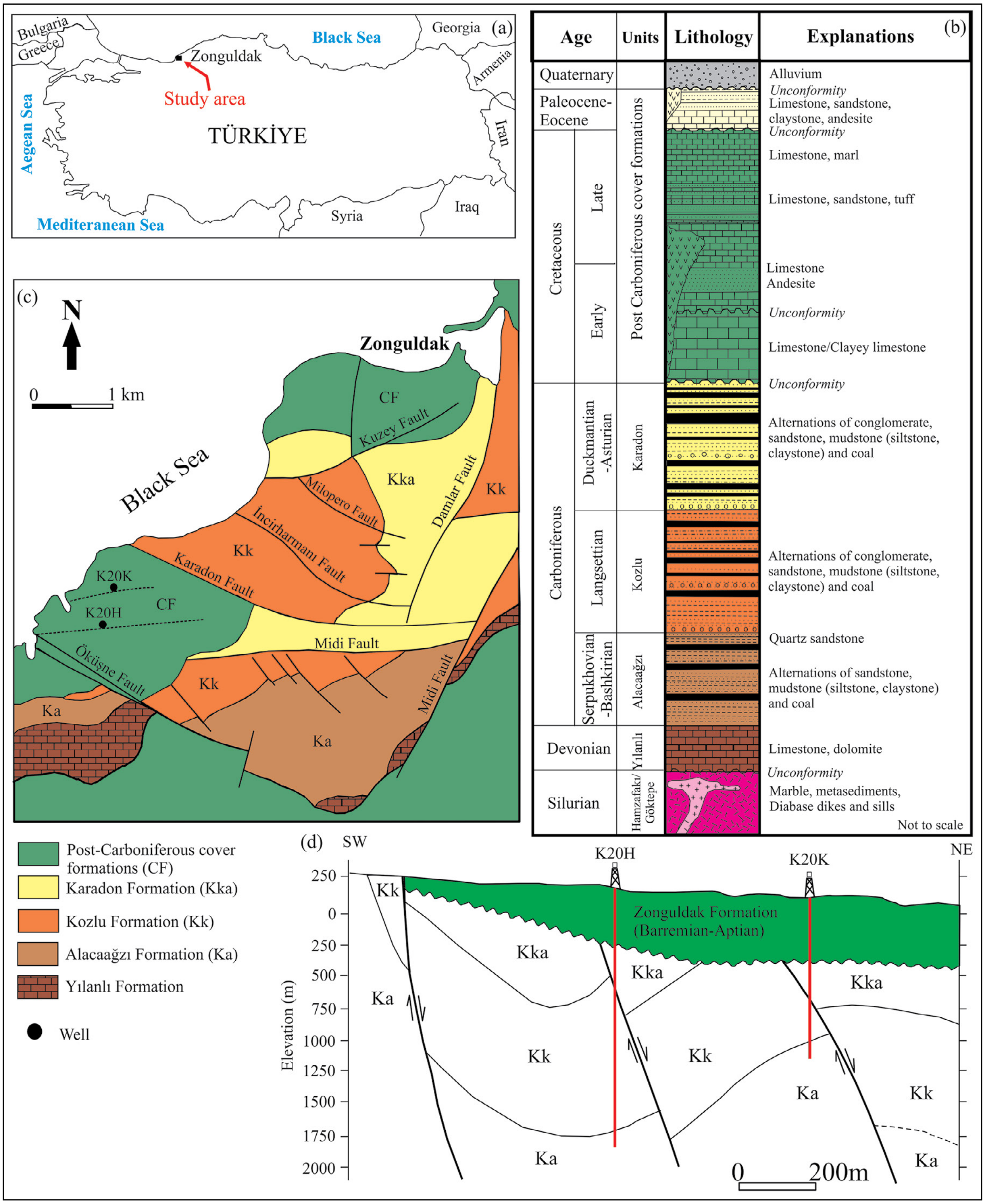

Figure 1- a) Location map of Zonguldak Basin, b) generalized stratigraphic column of surrounding area of the Kozlu coalfield, c) regional geological map of Zonguldak Basin, and d) simplified cross-section between studied wells (modified from Küskü et al., 1997; Yalçın et al., 2002; Karayiğit et al., 2018*a*).

1b). Previous sedimentological and palaeontological studies from the formation suggest that the formation was interpreted to have been deposited under mainly fluvial conditions (deltaic and meandering rivers) and lacustrine conditions during the Langsettian (Westphalian A) (Ağralı, 1970; Akyol, 1972; Kerey, 1985; Akgün and Akyol, 1992; Oktay, 1995; Yalçın et al., 2002; Cleal and Van Waveren, 2012; Opluštil et al., 2018). The Kozlu Formation is conformably overlain by the Karadon Formation (Figure 1b) and consists of alternations of conglomerate, sandstone, siltstone, claystone, and coal seams, as in the Kozlu Formation. This formation was deposited under fluvial conditions (deltaic and meandering river) and lacustrine conditions during the Duckmantian-Asturian (Westphalian B to D) (Ağralı, 1970; Kerey, 1985; Akgün and Akyol, 1992; Oktay, 1995; Yalçın et al., 2002; Cleal and Van Waveren, 2012; Opluštil et al., 2018).

Post-Carboniferous formations in the basin are mostly comprised of the Early Cretaceous Zonguldak Formation (Figure 1c and 1d) (Kerey, 1985; Karayiğit et al., 1998; Yalçın et al., 2002; Tüysüz et al., 2016). Even though the existence of coal clasts and coaly material were reported from the Zonguldak Formation (Mann et al., 1995; Yalçın et al., 2002), no coal seams were reported from this formation to date. The Zonguldak Formation is divided into four members, from bottom to top, lower Barremian Öküşne clastics member, Barremian Öküşne member, Early Aptian İnciğez clastics member, and Aptian Kapuz member (Küskü et al., 1997; Yalçın et al., 2002). The lower Barremian Öküşne clastics member composed of alternations of conglomerate, and sandstone-mudstone alternations, whereas Early Aptian İnciğez clastics members are alternations of conglomerate, sandstone, siltstone, claystone, and limestone. The Barremian Öküşne member is mainly made up of dolomitic limestone, and the Aptian Kapuz member is composed of sandy limestone and limestone. The orogenic movements from Hercynian to Alpine resulted in the development of several regional reverse faults and folds in the Zonguldak Basin (Figure 1c and 1d) (Okay et al., 1994; Yalçın et al., 2002; Okay and Nikishin, 2015). Thus, Carboniferous and Cretaceous sediments in the basin are deformed. Furthermore, post-Carboniferous dykes also intruded Carboniferous and Cretaceous formations in the basin (Karayiğit, 1992; Karayiğit et al., 1998; Yalçın et al., 2002).

3. Material and Applied Methodology

A total of fifty-four coal clast samples were obtained from different depths of the K20K and K20H research wells drilled at the Kozlu coalfield (Table 1). In this study, five coal clast samples (two from the K20K and three from the K20H) were examined from the Alacaağzı Formation; thirty-six coal clast samples (six from the K20K and thirty from the K20H) from the Kozlu Formation; twelve coal clast samples (four from the K20K and eight from the K20H) from the Karadon Formation; and only one coal clast sample from the limestone of the Early Aptian İnciğez clastics (Zonguldak Formation) was cored in the K20K well. The depths of identified formations in the K20H wells from bottom to top; 1891.00-2002.20-m Alacaağzı Formation, 715.30-1891.00-m Kozlu Formation, 424.70-715.3-m Karadon Formation, and 0-424.70-m Zonguldak Formation (287.00-424.70 Öküşne clastics and 0-287.00-m Öküşne limestone), while in the K20K well, 1119.90-1251.65-m Alacaağzı Formation, 793.05-1119.90-m Kozlu Formation, 468.70-793.05-m Karadon Formation, and 0-468.70 Zonguldak Formation (264.55-468.70-m Öküşne limestone, 203.00-264.55-m İnciğez clastics, and 0-203-m Kapuz limestone) (Figure 1d).

The fundamental petrographic observations of samples were conducted from polished coal blocks, which were prepared according to ASTM D2797/D2797M (2011) standard, under a reflected light microscope (Leica DM4000M coupled with J&M equipment and software) at Hacettepe University. The maceral identification was done according to the ICCP 1994 classification as modified by ICCP (1998 and 2001), and Pickel et al. (2017). The random vitrinite reflectance measurements (%Rr) were conducted mainly from collotelinite following the ISO 7404-5 (2009) standard using an oil-immersion 50X objective. The mineralogical compositions of suitable twenty-eight studied coal clast samples in both wells (one sample from the Zonguldak Formation, five samples from the Karadon Formation, eighteen samples from the Kozlu Formation, and four samples from the Alacaağzı Formation) were determined using an X-ray powder diffraction (XRD) with a Cu anode tube at Hacettepe University. In order to examine mineralogical compositions in detail, selected eight polished samples (K20K-O2, and -08, K20H-O1, -O5, -O7, -O15, -O39, and –O41) were coated with carbon and examined under Scanning Electron Microscope (SEM) equipped with Energy Dispersive X-Ray Analysis (EDX) in the General Directorate of Mineral Research and Exploration (MTA) and Hacettepe University.

Table 1- The list of coal clasts samples from K20K and K20H research wells and their depths and lithology of embedded sediment.

Well	Formation	Age	Sample No	Sampling depth (m)	Lithology of embedded sediment
K20K	Zonguldak (İnciğez clastics)	Early Aptian	K20K-O1	250.65	Pyritized limestone
	Karadon	Langsettian (Westphalian A)	K20K-O2	700.50	Conglomerate
			K20K-O3	710.50	Conglomerate
			K20K-O4	770.55	Conglomerate
			K20K-O5	789.15	Conglomerate
	Kozlu	Duckmantian-Asturian (Westphalian B-D)	K20K-O6	1030.10	Sandstone
			K20K-O7	1033.70	Conglomerate
			K20K-O8	1037.55	Conglomerate
			K20K-O9	1042.45	Conglomerate
			K20K-O10	1055.85	Conglomerate
			K20K-O11	1099.50	Sandstone
	Alacaağzı	Serpukhovian-Bashkirian (Namurian)	K20K-O12	1125.80	Conglomerate
			K20K-O13	1230.95	Conglomerate
K20H	Karadon	Langsettian (Westphalian A)	K20H-O1	431.70	Sandstone
			K20H-O2	451.00	Sandstone
			K20H-O3	455.40	Conglomerate
			K20H-O4	458.80	Conglomerate
			K20H-O5	527.30	Sandstone
			K20H-O6	541.00	Sandstone
			K20H-O7	636.20	Sandstone
			K20H-O8	686.30	Sandstone
	Kozlu	Duckmantian-Asturian (Westphalian B-D)	K20H-O9	754.80	Conglomerate
			K20H-O10	760.20	Conglomerate
			K20H-O11	813.40	Conglomerate
			K20H-O12	829.25	Conglomerate
			K20H-O13	1002.80	Conglomerate
			K20H-O14	1010.70	Conglomerate
			K20H-O15	1025.65	Conglomerate
			K20H-O16	1045.70	Sandstone
			K20H-O17	1061.30	Sandstone
			K20H-O18	1081.60	Sandstone
			K20H-O19	1101.80	Conglomerate
			K20H-O20	1118.30	Conglomerate
			K20H-O21	1136.20	Conglomerate
			K20H-O22	1141.40	Conglomerate
			K20H-O23	1146.80	Conglomerate
			K20H-O24	1162.20	Sandstone
			K20H-O25	1207.20	Claystone
			K20H-O26	1219.35	Sandstone
			K20H-O27	1244.60	Conglomerate
			K20H-O28	1281.30	Sandstone
			K20H-O29	1296.80	Conglomerate
			K20H-O30	1358.50	Sandstone
			K20H-O31	1447.00	Sandstone
			K20H-O32	1474.20	Conglomerate
			K20H-O33	1484.05	Conglomerate
			K20H-O34	1542.60	Conglomerate
			K20H-O35	1624.50	Conglomerate
			K20H-O36	1803.80	Conglomerate
			K20H-O37	1834.20	Sandstone
			K20H-O38	1850.00	Conglomerate
	Alaacağzı	Serpukhovian-Bashkirian (Namurian)	K20H-O39	1900.00	Sandstone
			K20H-O40	1972.30	Sandstone
			K20H-O41	1981.00	Pebbly sandstone

4. Findings

4.1. Macroscopic Description

The studied coal clast samples are variable in centimeter size (from 1 to 5 cm), and generally have surface areas around 1 cm^3 (Figure 2). The samples are mostly vitrinitic/xylitic and mostly dull bright sub-angular to angular and rarely rounded fragments and do not display any certain orientations (Figure 2). Furthermore, cleat/fracture carbonates were macroscopically observed in a few samples from the Late Carboniferous samples, and these cleat/fracture infillings are not observed in the coal clast-bearing embedded sediments. In contrast, cleat/fracture pyrite infillings are observed from the sample and embedded coal clast sample in the İnciğez clastics of the Zonguldak Formation. The investigated coal clast samples from the Late Carboniferous formations are mainly obtained from sandstone and conglomerate layers overlying coal seams, while one sample is obtained from a limestone bed within İnciğez clastics of the Zonguldak Formation.

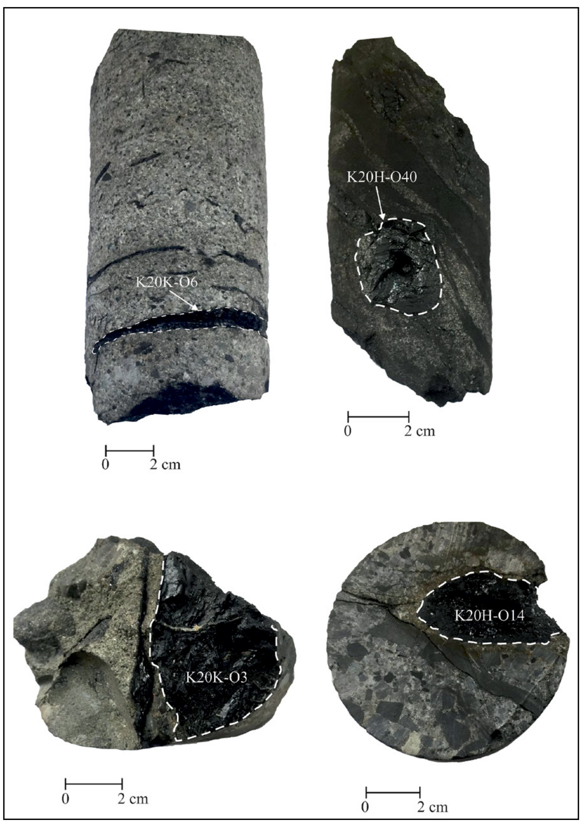

Figure 2- Selected photographs of the studied coal clast samples.

4.2. Coal petrography and Vitrinite Reflectance of Coal Clasts

The coal petrography examinations show that the majority of samples are composed only of vitrinite macerals, with liptinite and inertinite macerals rarely observed (Figures 3-7). Therefore, no detailed maceral counts were done from the studied clast samples. Collotelinite is the most common vitrinite maceral in all investigated samples (Figures 3b-f, 4a, 4b, 5a, 5b, 6a, 6b, and 7a, 7b), while telinite is more common in the xylitic/vitrinitic clast samples (Figures 3a-c and 5a). Collodetrinite and vitrodetrinite are other vitrinite macerals identified from the samples (Figures 3b, 4c and f, 5d, 6c, 6d, and 7a), while corpogelinite is identified in the clast sample from the Zonguldak Formation (Figure 3a). More importantly, deformed and/or brecciated vitrinite grains (Figures 3e, 4e, 5c, 5d, and 6a) and vitrinite with micro-cracks and -fissures (Figures 3e, 3f, 4b, and 5e) were observed in all studied formations. The existence of such grains could indicate that the peat slides during peat formation and/or mainly tectonic deformations during post-coalification (Taills, 1985; Xie et al., 2019; Hower et al., 2021). The latter possibility seems to be more common since the Carboniferous coal seams in the Zonguldak coalfield were deformed due to orogenic events (Yalçın et al., 2002; Okay and Nikishin, 2015; Karayiğit et al., 2018*a*). In addition, oxidized vitrinite grains with dark oxidation rims (Figures 7c and 7d) are observed in coal clasts from the Alacaağzı Formation samples, and vitrinite grains in clast samples from conglomerates of the Kozlu and Alacaağzı formations might also display possible brittle deformation around the clastic mineral matter (Figures 4f, 5f, and 6f).

Inertinite and liptinite macerals are embedded within collodetrinite (Figures 4a-d, 5b, 5c, and 6c, 6d), as reported in the coal seams in both wells (Karayiğit et al., 2018*a*). Fusinite, semifusinite, macrinite, and inertodetrinite are the generally observed inertinite group macerals, while micrinite bands within collodetrinite are also identified in some samples (Figures 4a-c, 5b, 5d, and 6c, 6d). Similar to the Kozlu and Karadon formations in the studied wells and Amasra coalfield (Karayiğit et al., 2018*a, b*), sporinite is commonly identified in the studied samples (Figure 4a, 4c, and 4d), and cutinite is also rarely identified. In the Karadon Formation, liptinite

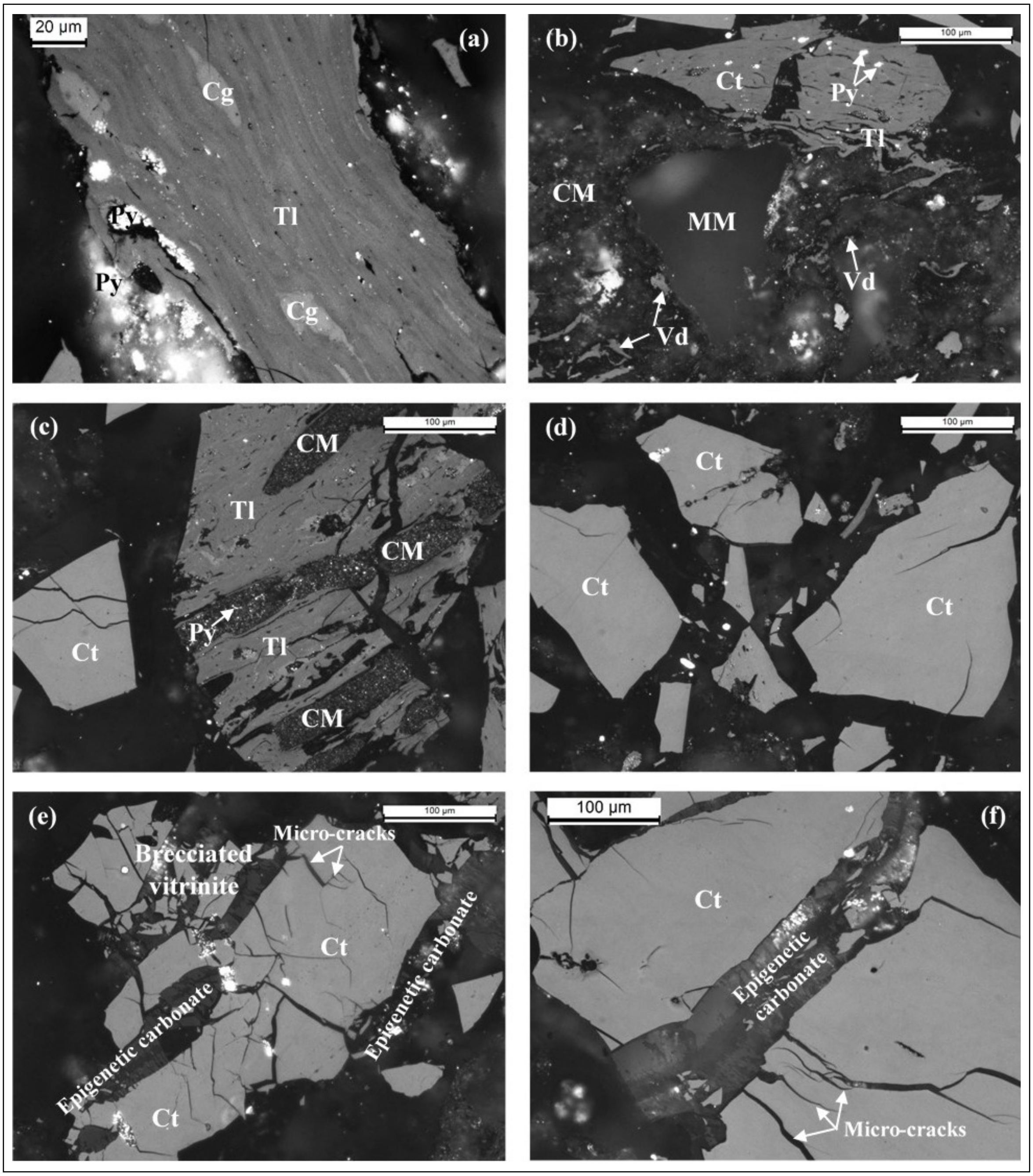

Figure 3- Selected microphotographs of clast sample (K20K-O1) from the Zonguldak Formation; a) tellinite (Tl) and cell-lumen infilling corpogellinite (Cp), and framboidal pyrite (Py) grain; b) tellinite (Tl), framboidal pyrite (Py) grains within collotellinite (Ct), and vitrodetrinite (Vd) and mineral matter (MM) within clay mineral (CM) matrix, c) collotellinite (Ct), and tellinite (Tl) and cell-lumen infilling clay mineral (CM) and pyrite (Py), d) collotelinite (Ct), e) and f) epigenetic carbonate cleat/fracture infilling between micro-cracks-bearing collotelinite (Ct) and brecciated vitrinite grains. All photomicrographs are taken under incident white light and oil immersion, 500 × total magnification. The %Rr value of the sample is 1.01%±0.02.

macerals, particularly sporinite, in some samples display a very weak fluorescent colour under blue-light excitation (Figures 4c, 4d), while in the Kozlu Formation sporinite shows a pale grey colour under incident light (Figure 5c). The cleat/fracture carbonate mineral-infillings are commonly identified in between the brecciated vitrinite grains (Figures 3e, 3f, 4e, and 7c), which was also commonly reported from coal seams in the studied wells by Karayiğit et al. (2018*a*). In addition, cleat/fracture pyrite-infillings

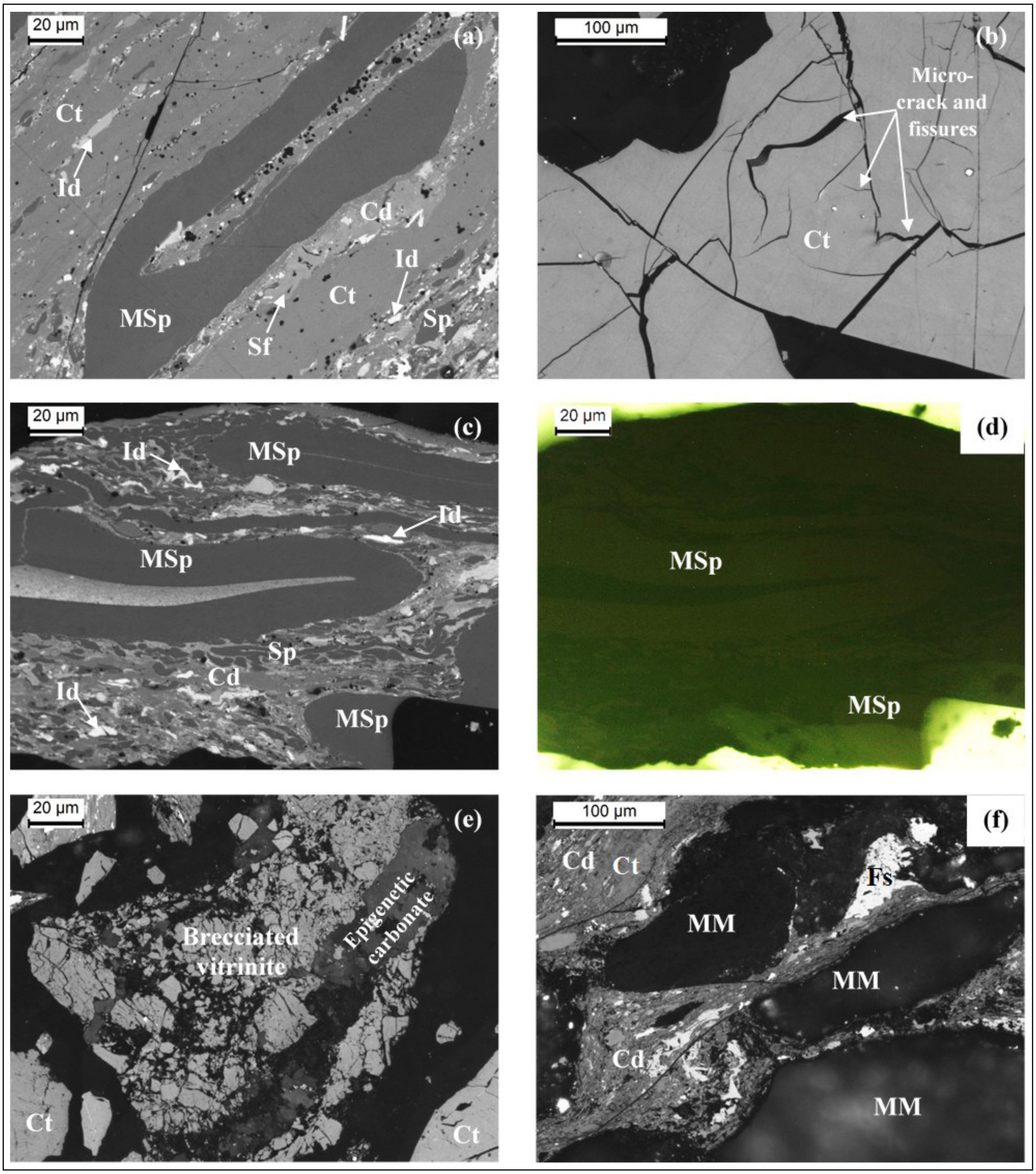

Figure 4- Selected microphotographs of clast samples from the Karadon Formation; a) intertodetrinite (Id), semifusinite (Sf), mega-sporinite (Msp) and sporinite (Sp) embedded within collodetrinite (Cd) and collotelinite (Ct), b) micro-cracks and -fissures within collotelinite (Ct), c) and d) intertodetrinite (Id), mega-sporinite (Msp) and sporinite (Sp) embedded within collodetrinite (Cd), e) epigenetic carbonate mineral-infillings between brecciated vitrinite and collotelinite (Ct), f) collodetrinite (Cd) mineral-matter (MM) and fusinite (Fs) within display plastic deformation. All photomicrographs are taken under incident white light (a, b, c, e and f) and blue-light excitation (c), oil immersion, 500 × total magnification. Images a, c, and d from K20H-O3 (%R_r=0.94±0.02), b from K20H-O1 (%R_r=0.98±0.02), e and f from K20H-O7 (%R_r=0.99±0.02).

and pyritized macerals were also detected in some samples. Other identified minerals using white incident light under a coal petrography microscope are framboidal pyrite grains (Figures 3a and 7a), and rarely clay mineral aggregates (Figure 3b, 3c, and 7a) and syngenetic carbonate minerals (Figures 7a, 7b). In the Alacaağzı Formation, a few flake graphite grains were identified (Figures 7e, 7f). Considering

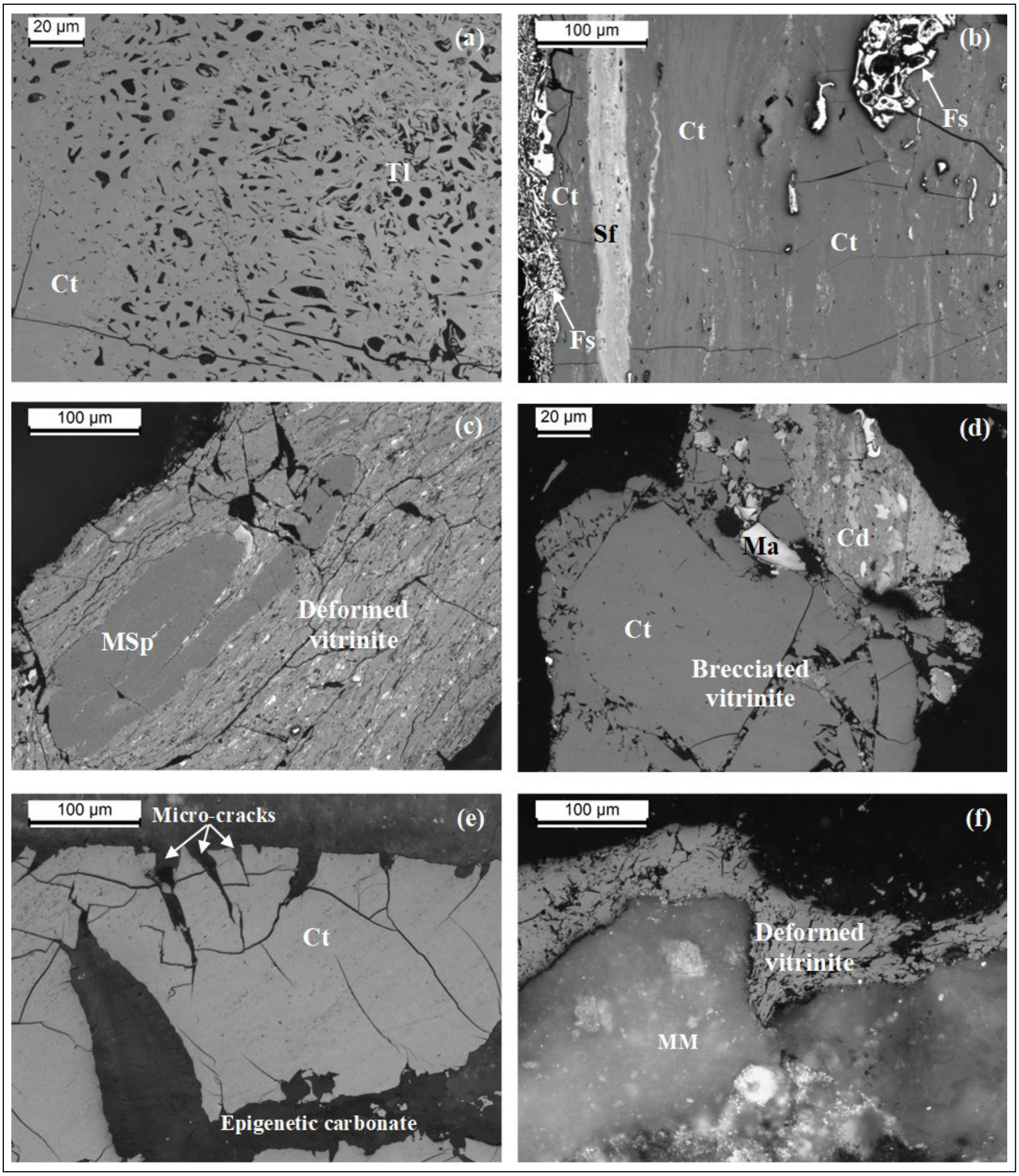

Figure 5- Selected microphotographs of clast samples from the Kozlu Formation; a) tellinite (Tl) and collotellinite (Ct), b) collotelinite (Ct), fusinite (Fs) and semifusinite (Sf), c) deformed vitrinite and mega-sporinite (Msp) grain;, d) collodetrinite (Cd), macrinite (Ma), collotelinite (Ct), and brecciated vitrinite grains, e) micro-cracks-bearing collotelinite (Ct) and epigenetic carbonate cleat/fracture infilling, f) deformed vitrinite around mineral matter (MM). All photomicrographs are taken under incident white light and oil immersion, 500 × total magnification. Images a and b from K20K-O7 (%R_r=1.26±0.02), c from K20H-O10 (%R_r=1.06±0.03), d from K20H-O33 (%R_r=1.32±0.03), e from K20K-O8 (%R_r=1.28±0.03), f from K20H-O22 (%R_r=1.23±0.03).

the lack of thermal impact and natural coke formation in the studied wells, the graphite grains were derived as clastic inputs into parental coal seams from presumably Silurian Hamzafakı Formation and/or Devonian Göktepe Formation, where metasediments were intruded with magmatic dykes (Küskü et al., 1997; Karayiğit et al., 2018*a*).

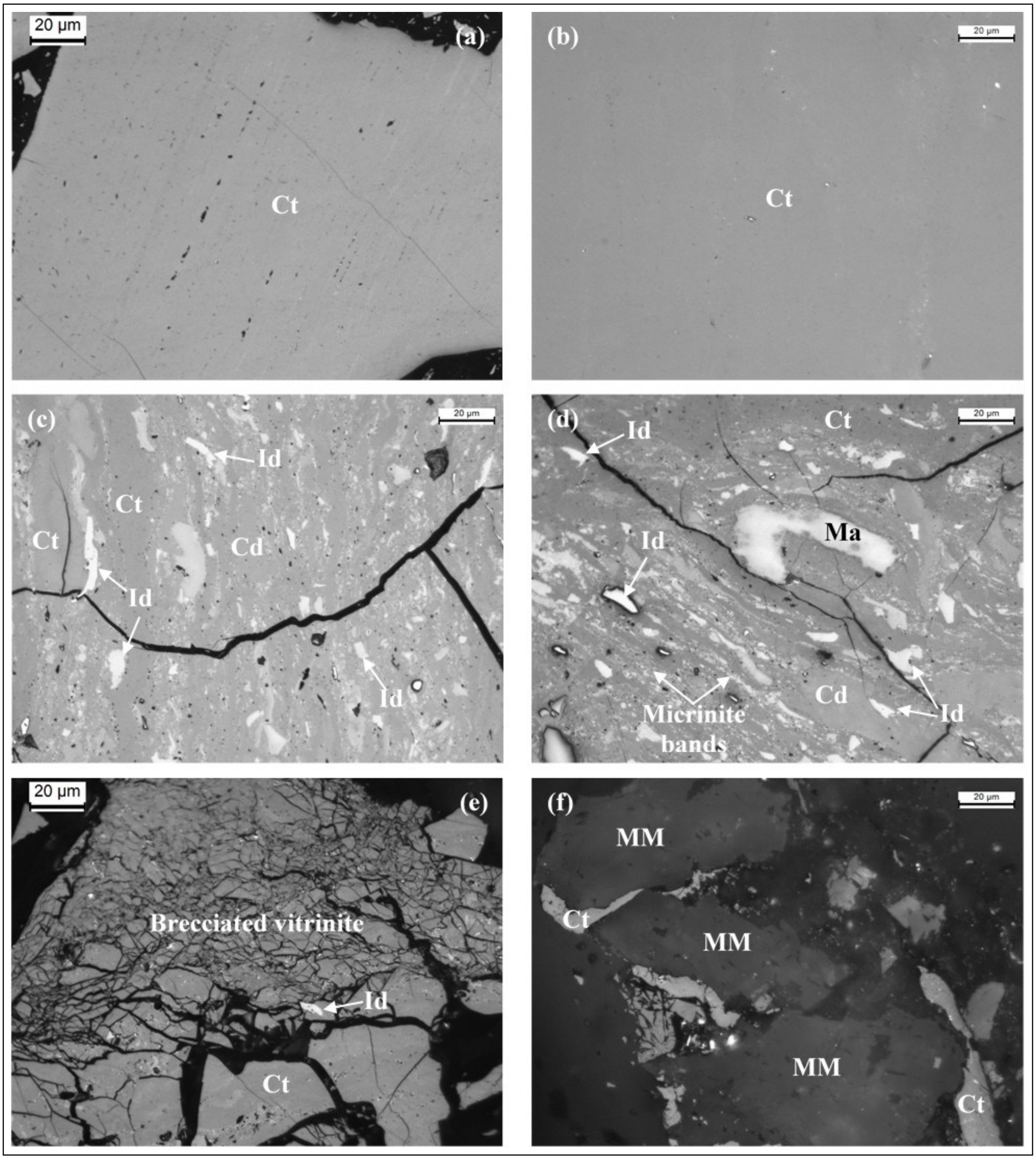

Figure 6- Selected microphotographs of clast samples from the Alacaağzı Formation; a), b) collotelinite (Ct), c), d) collodetrinite (Ct), and inertodetrinite (Id), macrinite (Ma) and micrinite bands embedded within collodetrinite (Cd), e) deformed collotellinite (Ct) around mineral-matter (MM), f) collotelinite (Ct), inertodetrinite (Id) and brecciated vitrinite grains. All photomicrographs are taken under incident white light and oil immersion, 500 × total magnification. Images a and c from K20H-O41 (%R_r=1.73±0.03), b from K20K-O12 (%R_r=1.29±0.02), d and e from K20K-O13 (%R_r=1.29±0.03), f from K20H-O40 (%R_r=1.72±0.03).

The %Rr values of coal clast samples from the Alacaağzı Formation show significant differences between K20H (1.70%-1.72%±0.03) and K20K (1.29%±0.02) wells (Table 2). The samples of the Kozlu Formation in the K20H well have %Rr values of 1.08-1.31±0.02, while the %Rr values of samples obtained from this formation in the K20K well display a wide range and vary from 1.04±0.02 to 1.52±0.03 (Table 2). The Karadon Formation samples cored in the K20K well have %Rr values ranging from

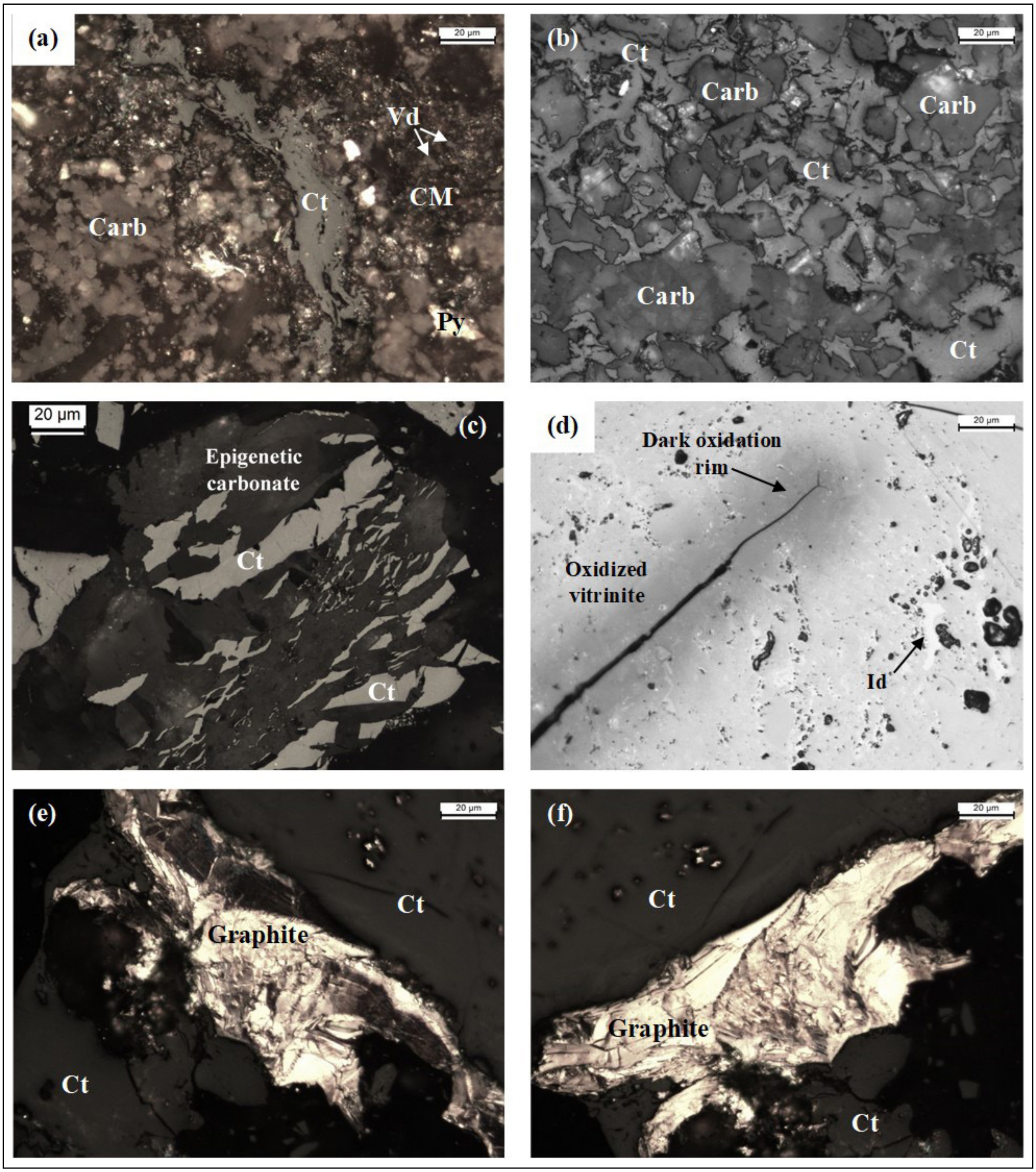

Figure 7- Selected microphotographs of clast samples from the Alacaağzı Formation; a) collotelinite (Ct) and vitrodetrinite (Vd) within clay mineral (CM) matrix, syngenetic carbonate (Carb) grains, and pyrite (Py), b) collotelinite (Ct) and carbonate (Carb) grains; c) oxidized vitrinite with dark oxidation rim and inertodetrinite (Id), d) epigenetic carbonate cleat/fracture infillings between brecciated collotelinite (Ct) grains, and e), f) clastic graphite grain, possibly derived from pre-Carboniferous basement, and collotelinite (Ct). All photomicrographs are taken under incident white light (a-d) and partially crossed polarizers (e-f), oil immersion, 500 × total magnification. Images from a, b, d-f from K20K-O13 (%R_r=1.29±0.03), c from K20H-O40 (%R_r=1.72±0.03).

1.02-1.05±%0.03, whereas the %Rr values of samples of this formation from the K20H well are almost within the range of standard derivation of ones from the K20H well and vary from 0.94%±0.02 to 1.06%%±0.02 (Table 2). Finally, the %Rr value of a coal clast sample (K20K-O1) from the Early Aptian İnciğez clastics is 1.01±0.02 (Table 2).

Table 2- The random reflectance (%Rr) of collotelinite and standard deviation (Stdv) of coal clasts samples from K20K and K20H research wells.

Well	Formation	Age	Sample No	%Rr ± Stdv
K20K	Zonguldak	Early Aptian	K20K-O1	1.01±0.02
	Karadon	Langsettian (Westphalian A)	K20K-O2	1.05±0.02
			K20K-O3	1.05±0.02
			K20K-O4	1.05±0.02
			K20K-O5	1.02±0.02
	Kozlu	Duckmantian-Asturian (Westphalian B-D)	K20K-O6	1.08±0.02
			K20K-O7	1.26±0.02
			K20K-O8	1.28±0.03
			K20K-O9	1.31±0.03
			K20K-O10	1.18±0.03
			K20K-O11	1.19±0.02
	Alacaağzı	Serpukhovian-Bashkirian (Namurian)	K20K-O12	1.29±0.02
			K20K-O13	1.29±0.03
K20H	Karadon	Langsettian (Westphalian A)	K20H-O1	1.04±0.03
			K20H-O2	0.98±0.02
			K20H-O3	0.94±0.02
			K20H-O4	0.99±0.03
			K20H-O5	1.00±0.03
			K20H-O6	1.00±0.02
			K20H-O7	0.99±0.02
			K20H-O8	1.06±0.02
	Kozlu	Duckmantian-Asturian (Westphalian B-D)	K20H-O9	1.04±0.02
			K20H-O10	1.06±0.03
			K20H-O11	1.06±0.02
			K20H-O12	1.10±0.02
			K20H-O13	1.16±0.03
			K20H-O14	1.18±0.02
			K20H-O15	1.15±0.02
			K20H-O16	1.19±0.02
			K20H-O17	1.15±0.02
			K20H-O18	1.28±0.02
			K20H-O19	1.28±0.03
			K20H-O20	1.19±0.03
			K20H-O21	1.22±0.02
			K20H-O22	1.23±0.03
			K20H-O23	1.24±0.03
			K20H-O24	1.31±0.02
			K20H-O25	1.30±0.02
			K20H-O26	1.20±0.02
			K20H-O27	1.26±0.03
			K20H-O28	1.25±0.03
			K20H-O29	1.27±0.03
			K20H-O30	1.31±0.02
			K20H-O31	1.42±0.02
			K20H-O32	1.32±0.03
			K20H-O33	1.32±0.03
			K20H-O34	1.41±0.02
			K20H-O35	1.49±0.03
			K20H-O36	1.54±0.02
			K20H-O37	1.54±0.02
			K20H-O38	1.52±0.03
	Alaacağzı	Serpukhovian-Bashkirian (Namurian)	K20H-O39	1.70±0.03
			K20H-O40	1.72±0.03
			K20H-O41	1.73±0.03

4.3. Mineralogy of Coal Clasts

The XRD results show that analysed coal clast samples from all studied formations display similar mineralogical compositions (Table 3). Quartz is detected as a generally abundant to dominant phase, while clay minerals (kaolinite and illite/mica) and feldspar are minor phases in the samples (Table 3). As expected, calcite is a dominant phase in the cleat/fracture carbonate-infillings-bearing samples, and dolomite and ankerite are detected as minor phases in these samples (Table 3). Siderite is found in one sample (K20K-O13) from the Alacaağzı Formation (Table 3). Pyrite is an abundant phase in the samples from the Zonguldak Formation, while it is found as a minor phase in some samples from the Karadon and Kozlu formations (Table 3). Besides XRD analysis, anglesite, apatite, barite, chalcopyrite, chlorite (chamosite), galena, monazite, sphalerite, titanite/sphene, Ti-oxides, and zircon are detected as accessory minerals according to the SEM-EDX data (Table 3).

5. Discussion

5.1. Origins of Minerals

The petrographical and SEM examinations indicate that minerals in the coal clast samples are derived from the parental Carboniferous coal seams and the precipitation of solutions cleats/fractures of coal clasts after the diagenesis of embedded sediments and early coalification of parental coal seams. Quartz, like in Carboniferous coal seams in the studied wells, is generally identified as individual grains within clay mineral matrices during SEM examination (Figures 8a, 8d, 8e, 8f, 9a and 10b). These grains are clearly derived as clastic inputs into palaeomires of parental coal seams. Clay mineral matrices associated with individual quartz, feldspars, apatite, monazite, titanite/sphene, and zircon grains and organic matter (macerals) were observed, and the SEM-EDX data showed that the matrices have mostly kaolinite and illitic compositions (Figures 8a-f and 10a-b). Similar associations within kaolinite matrices were also reported from the coal seams in the studied wells and other coalfields in the Zonguldak Basin (Karayiğit et al., 2018*a, b*), and also from tonstein layers in the Zonguldak Basin (Burger et al., 2000), which were formed from alteration of synchronous and/or epiclastic volcanic inputs within palaeomires during the Carboniferous. Hence, the identified kaolinite matrices and associated minerals from the investigated coal clast samples are derived from parental coal seams. Illitic matrices are presumably derived as clastic influx into palaeomires of the parental coal seams; nevertheless, these matrices might also be originated from the transformation of clastic smectite and/or interstratified illite/smectite matrices into illite during the diagenesis of embedded sediments. Besides, cleat/fracture kaolinite-infillings were also observed in some samples (Figures 9a-e). Since cleat/fracture kaolinite-infillings were observed as monomineral infilling or accompany with sulphide minerals (pyrite and galena), these infillings seem to be formed from the precipitation of Al and Si-rich hydrothermal solutions during either the early coalification stage of the parental seams, as like coal seams in both wells (Karayiğit et al., 2018*a*), or more possible during the diagenesis of embedded sediments.

Carbonate minerals are mainly identified as individual grains (Figures 8a and 10a) and nodules (Figures 8c and 10b) within clay mineral matrices, and more commonly cleat/fracture infillings (Figures 9f and 10c-f), particularly from deformed and brecciated vitrinite grains-bearing samples.

These infillings are mostly calcite with detectable Mg and pure dolomite (Figures 10c-f), and, to a lesser extent, Fe-rich dolomite with measurable Mn (Figures 10e and 10f) and ankerite (Figures 9f and 10c). Such carbonate mineral-infillings are commonly reported in Permo-Carboniferous coals and mostly originate from the precipitation of Ca-rich hydrothermal solutions (Dawson et al., 2012; Permana et al., 2013; Xie et al., 2019; Valentim et al., 2020).

In accordance with this, Karayiğit et al. (2018*a*) also assumed that these carbonate infillings are related to the precipitation of Ca-rich solutions derived by penetration of hydrothermal solutions or leached solutions from overlying Early Cretaceous limestones *via* fault zones into coal seams in the studied wells. Considering the presence of carbonate infillings between deformed and brecciated vitrinite grains in the studied samples, Ca-rich solutions could either have penetrated after the tectonic deformation of parental

Table 3- Minerals identified in the analyzed coal clast samples based on XRD and SEM-EDX analyses (+++ = dominant phase, ++ = abundant phase, + = minor phase by XRD, a: by SEM-EDX; Abbrevations: CM: clay minerals, Feld: feldspars, Ank/Dol: ankerite/dolomite, Mnz/Ap: monazite/apatite).

Well	Formation	Sample No	Quartz	CM	Feld	Titanite	Calcite	Ank/Dol	Siderite	Pyrite	Chalcopyrite	Galena	Sphalerite	Ti-oxides	Mnz/Ap	Barite	Anglesite	Zircon
K20K	Zonguldak	K20K-O1	+++	+			+	+		++								
	Karadon	K20K-O2	++	a			+	a										
		K20K-O3	++	+			+	++		+								
		K20K-O4	+++	+			+++	+										
		K20K-O5	+	+														
	Kozlu	K20K-O7	+					++										
		K20K-O8	a				a	a						a				
		K20K-O9	++				+	+										
		K20K-O10	+	+			+											
		K20K-O11	+++	++	+													
	Alacaağzı	K20K-O12	++	+				+										
		K20K-O13	+++	+	+		+		+									
K20H	Karadon	K20H-O1	a	a			a	a		a		a					a	
		K20H-O4	+	+++			+	+		+								
		K20H-O5	a	a						a		a	a					
		K20H-O7	a	a	a		a	a		a	a				a			
	Kozlu	K20H-O10	+++	++														
		K20H-O12	+	+			+++											
		K20H-O15	+++	+			++	+		+	a		a			a		a
		K20H-O19	+++	++	+													
		K20H-O20	++	+	+		+											
		K20H-O21	+	+														
		K20H-O22	+++	+++	+		+											
		K20H-O25	++	+			+											
		K20H-O26	+	++														
		K20H-O27	+	++			+++	+++		+								
		K20H-O28	+	+														
		K20H-O30	++	+			+	+		+								
		K20H-O32	+++	++														
		K20H-O33	+++	++	+		+++											
		K20H-O34	+	+	+													
	Alacaağzı	K20H-O39	+	a				+		a				a		a		a
		K20H-O40	++	+	+			++										
		K20H-O41	a	a	a	a	a	a	a	a	a			a	a			a

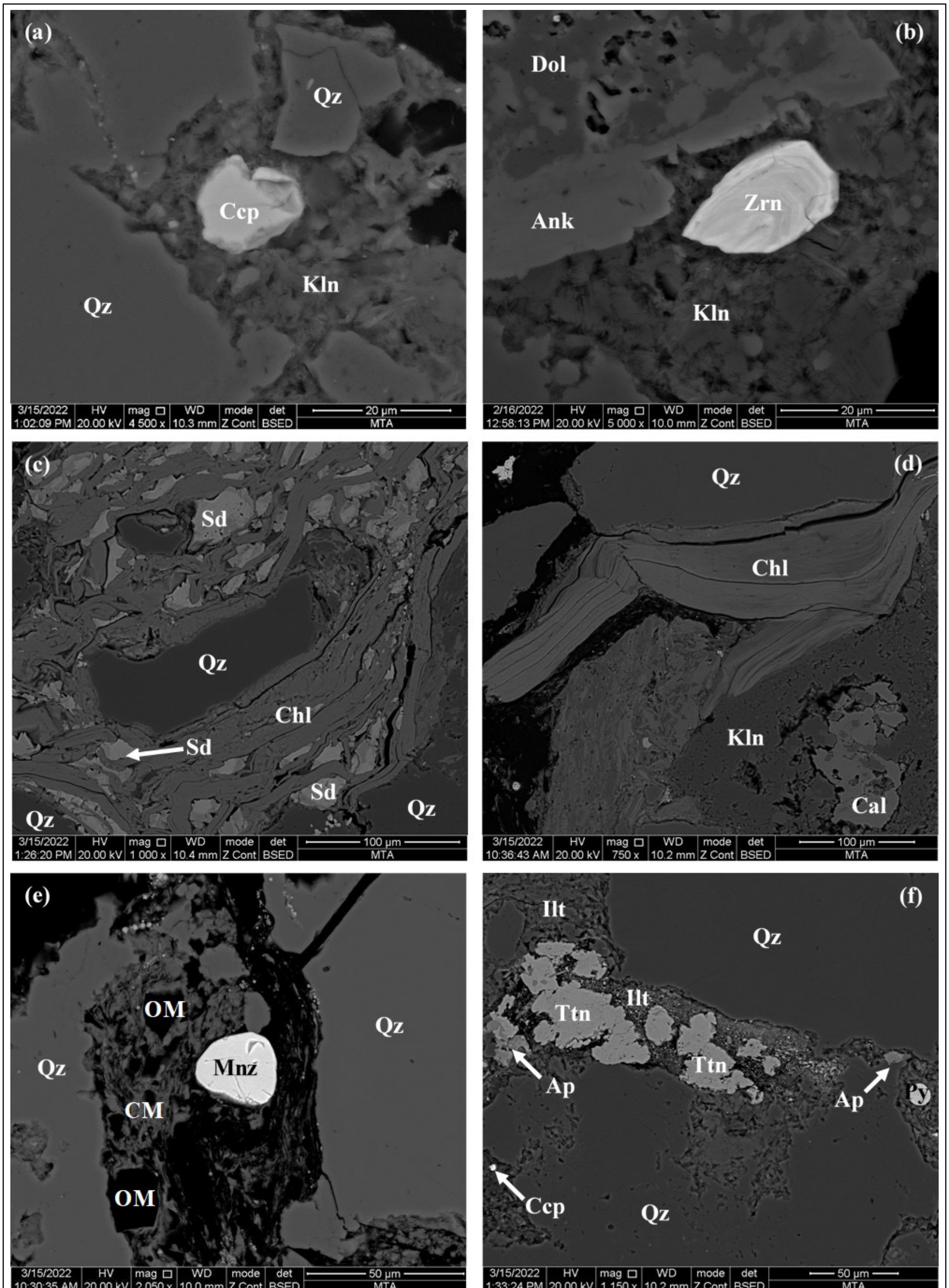

Figure 8- Selected SEM backscattered electrons (SEM-BSE) images; a), b) and d) ankerite (Ank), calcite (Cal), chlorite (Chl), chalcopyrite (Ccp), dolomite (Dol), quartz (Qz) and zircon (Zr) grains within kaolinitic (Kln) matrix, c) chlorite (Chl) associated with siderite (Sd) nodules and quartz (Qz) grains, e) monazite (Mnz) and quartz (Qz) grains and organic matter (OM) associated with clay mineral (CM), f) apatite (Ap), chalcopyrite (Ccp), quartz (Qz) and titanite (Ttn) grains within illitic (Ilt) matrix. Images a from K20H-O15, b and f from K20H-O41, d and e from K20H-O7.

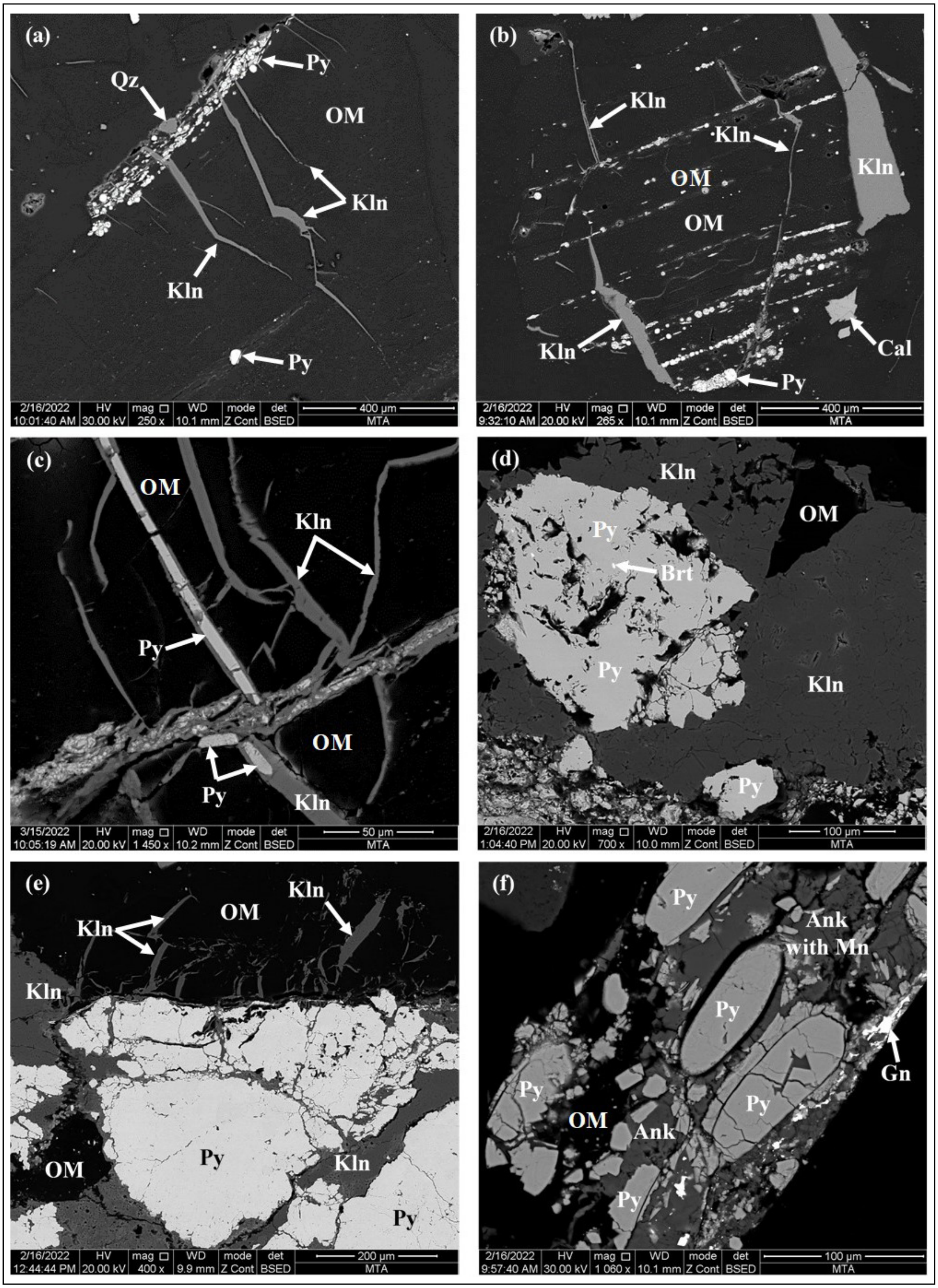

Figure 9- Selected SEM-BSE images; a), b) cleat/fracture kaolinite (Kln)-infillings within organic matter (OM), syngenetic framboidal pyrite (Py) grains and calcite (Cal) grains, c) cleat/fracture kaolinite (Kln) and pyrite (Py)-infillings within organic matter (OM), d) and f) cleat/fracture barite (Brt), pyrite (Py) and kaolinite (Kln)-infillings within organic matter (OM), e) cleat/fracture galena (Gn), pyrite (Py) and ankerite (Ank) with measurable Mn-infillings within organic matter (OM). Images a, b, e from K20H-O1, c from K20H-O7, d and f from K20H-O15.

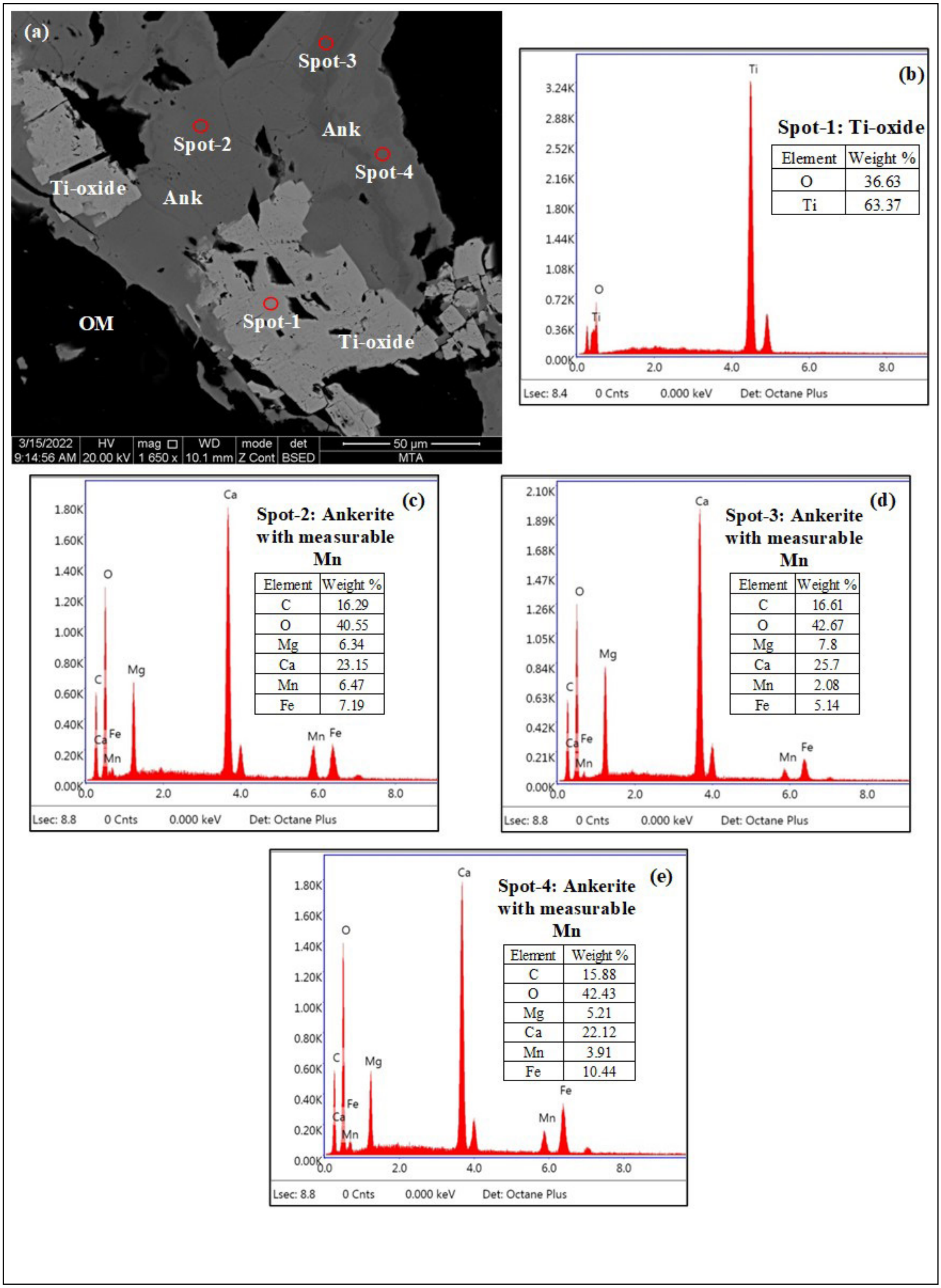

Figure 10- Selected SEM-BSE images; a) ankerite (Ank), dolomite (Dol) and zircon grains within illitic (Ilt) matrix, and cleat/fracture kaolinite (Kln)-infilling within organic matter (OM), b) siderite (Sd) nodule, plagioclase (Pl) and quartz (Qz) within illitic (Ilt) matrix, c), d) cleat/fracture ankerite (Ank), calcite (Cal) and quartz/silica (Qz)-infillings within organic matter (OM), e) and f) cleat/fracture calcite (Cal), dolomite (Dol) and Ti-oxide-infillings within organic matter (OM). Images a and c from K20H-O15, b from K20H-O41, d from K20H-O7, e and f from K20K-O8.

coal seams or embedded sediments. Nevertheless, the presence of carbonate-infillings in clast samples might also have originated from the precipitation of Ca-rich intra-formation solutions during the diagenesis of embedded limestone in case of the Zonguldak Formation or penetration of carbonate cement of conglomerate for Carboniferous clast samples. Nevertheless, the latter case was probably not common due to the lack of carbonate mineralization around Carboniferous coal clasts. Siderite nodules were detected rarely in a few samples within organic matter or clay matrices (Figure 8c and 10b), which implies these nodules originated from the parental coal seams and formed within palaeomires (Karayiğit et al., 2017, 2018*a, b*; Dai et al., 2020). The formation of epigenetic Ti-oxide (anatase/rutile)-infillings in coals is mostly controlled by the precipitation of hydrothermal solutions (Zhao et al., 2018; Rodrigues et al., 2020; Liu et al., 2021). In the samples from the Kozlu Formation, cleat/fracture Ti-oxide infillings are associated with carbonate mineral-infillings (Figures 10f and 11). Such infillings were also developed from the precipitation of hydrothermal solutions.

Framboidal pyrite grains within organic matter are clearly related to parental coal seams (Figures 3a, 7a, 9a, 9b, and 12a). These framboidal pyrite grains formed authigenically within the palaeomires or early diagenesis of parental coal seams. The cleat/fracture pyrite-infillings were also commonly reported from the coal seams in the basin (Karayiğit et al., 1998, 2018*a, b*), which were formed after the precipitation of Fe- and sulfate-rich from penetrated hydrothermal solutions during coalification. Similar cleat/fracture pyrite-infillings are also identified from the Carboniferous coal clasts (Figures 9c-f), which were also derived from the precipitation of penetrated hydrothermal solutions, as like the kaolinite and carbonate minerals. Even though the determination of the timing of penetration of such solutions could not be estimated accurately, these pyrite-infillings were presumably formed mainly during the diagenesis of embedded coal seams and, to a lesser extent, during the early coalification of parental coal seams. Considering the presence of macroscopically identified cleat/fracture pyrite-infillings in the Early Aptian coal clast sample, pyritized macerals and cleat/fracture pyrite-infillings in this sample seem to have developed within the depositional environment during the Early Aptian and/or post-Aptian. Besides the cleat/fracture pyrite-infillings and framboidal pyrite grains, galena and chalcopyrite are other identified sulphide minerals in the samples. Galena is only identified as cleat/fracture infillings, and such infillings are generally accompanied by carbonate minerals (Figures 9f and 12) and kaolinite (Figure 13). Chalcopyrite is only observed as individual grains within clay mineral matrices (Figure 8a and f), which imply a clastic origin for such grains. Barite (Figure 9d) and anglesite (Figure 14) are also only detected as cleat/fracture infillings. Barite seems to have been formed either during the early coalification of parental coal seams and/or diagenesis of embedded sediments. The anglesite overgrowths around galena-infillings, which grew after galena formation, formed due to the alteration of galena-infillings by pore-waters or hydrothermal solutions after galena formation.

Although mono-mineralic cleat/fracture infillings (e.g., Figures 9a, 9b and 10c) are commonly observed in the samples, multi-mineralic (e.g., carbonate-sulphide minerals or kaolinite-sulphide minerals) infillings are also detected (e.g, Figures 9c-f, 10d-f, 11a, and 13), like coal seams in the studied wells. Such multi-mineralic mineral infillings also formed from the precipitation of hydrothermal solutions in coal (Hower et al., 2001; Dawson et al., 2012; Permana et al., 2013; Karayiğit et al., 2018*a*; Liu et al., 2021); thus, these infillings might be derived from the mainly precipitation during mainly within parental coal seams and/or diagenesis of embedded sediments, particularly for coal clast sample from the Zonguldak Formation.

5.2. Ranks and Origins of Coal Clasts

The rank and grade determination of coal seams are based on a combination of several parameters (e.g., %Rr, gross calorific values, and ash yields); however, the size of investigated coal clast grains did not permit all desired proximate, ultimate, and calorific analyses for rank and grade determination. Therefore, the rank determination of the investigated samples is only based on %Rr values. The %Rr values of coal clasts of the Alacaağzı Formation, as mentioned previously, display differences (Table 2 and Figure 15);

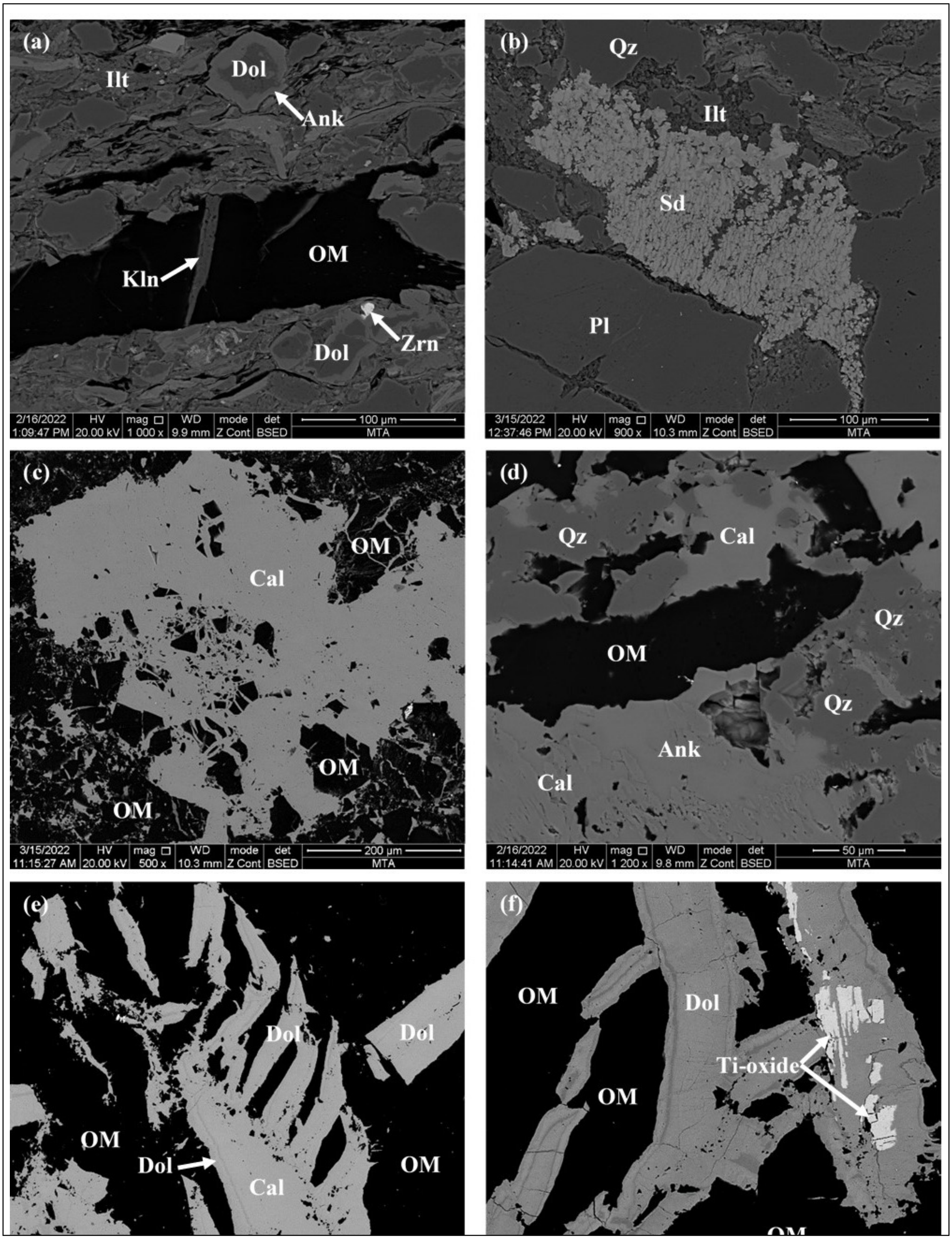

Figure 11- a) SEM-BSE image of cleat/fracture ankerite (Ank) and Ti-oxide-infillings within organic matter (OM), b) SEM-EDX spectra of Ti-oxide at spot-1 and c), d) ankerite with measurable Mn at spot-2. Image from K20K-O8.

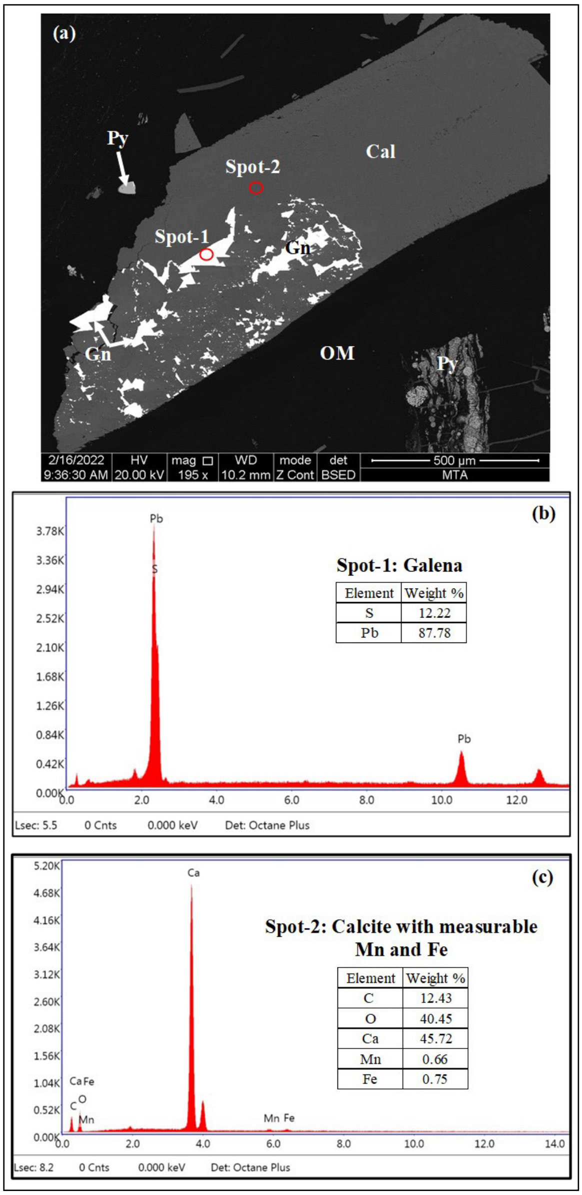

Figure 12- a) SEM-BSE image of cleat/fracture calcite (Cal) and galena (Gn)-infillings within organic matter (OM) and pyrite (Py), b) SEM-EDX spectra of galena at spot-1 and c) calcite with measurable Mn and Fe in image a. Image from K20H-O1.

thus, the samples of this formation have relative rank differences. Furthermore, the %Rr values of coal clasts could be very useful for determining the origin of coal clasts since coal clasts generally do not display diagenesis differences with parental coal seams (Gayer et al., 1996; Kožušníková et al., 1999; Daněk et al., 2002; Pešek and Sýkorová, 2006; Misz-Kennan et al., 2019). Of note, in some cases, coal clasts could display a lower rank than the parental coal seams. The samples from the K20H well are of bituminous A (medium rank A) according to ISO 11760 (2005) coal-rank classification, while samples obtained from the K20K well are of bituminous B (medium rank B). This difference is not surprising since the Alacaağzı Formation in the K20H well was cored to deeper depths than the K20K (Figures 1d and 15a), and %Rr values of coal seams in the Alacaağzı Formation in the K20H well are relatively higher than coal seams in the K20K well (Karayiğit et al., 2018*a*). Furthermore, the %Rr values of the Alacaağzı coal clasts samples in the K20K are relatively higher than the coal seams in this well (Table 1 and Figure 15b), but the %Rr values are still within the range of standard deviation and close to the %R_{max} values of coal seams in the Alacaağzı Formation (Table 4). This difference could be controlled by the oxidation of clast samples during the transportation since micro-crack and –fissures-bearing vitrinite grains and oxidized vitrinite grains were observed in these samples. All these could imply that the erosion of paternal coal seams seems to take place during the peat stage and/or early stages of coalification and transportation of coal clasts sample took place in a short distance, while oxidation of coal clasts was limited.

In contrast with the K20K well (1.29%±0.02), the %Rr values of coal clast (1.70-1.73%±0.03) from the Alacaağzı Formation in the K20H are slightly higher than coal seams (1.48-1.52%) of the Alacaağzı Formation cored in this well (Table 4 and Figure 15a). This difference might be related to oxidation clast during transportation; however, this explanation could be applicable to sample K20H-O39, which was obtained from sandstone between two coal seams, and the remaining Alacaağzı clast samples were obtained from conglomerate and sandstone layers beneath the coal seams in this well. This could easily suggest that the burial depth might increase their %Rr values, but the theoretically calculated %Rr values (1.48-1.52 %Rr) using the depth of these clasts (1900-1981 m beneath the surface) are close to the overlying coal seams (Figure 15a). Hence, burial depth impact might be limited on the coalification of these clast samples. These samples are also characterized by the presence of deformed and brecciated vitrinite grains (Figures 6e, 6f, and 7e). Previous palynological and palaeobotanical data from the coal-bearing formations

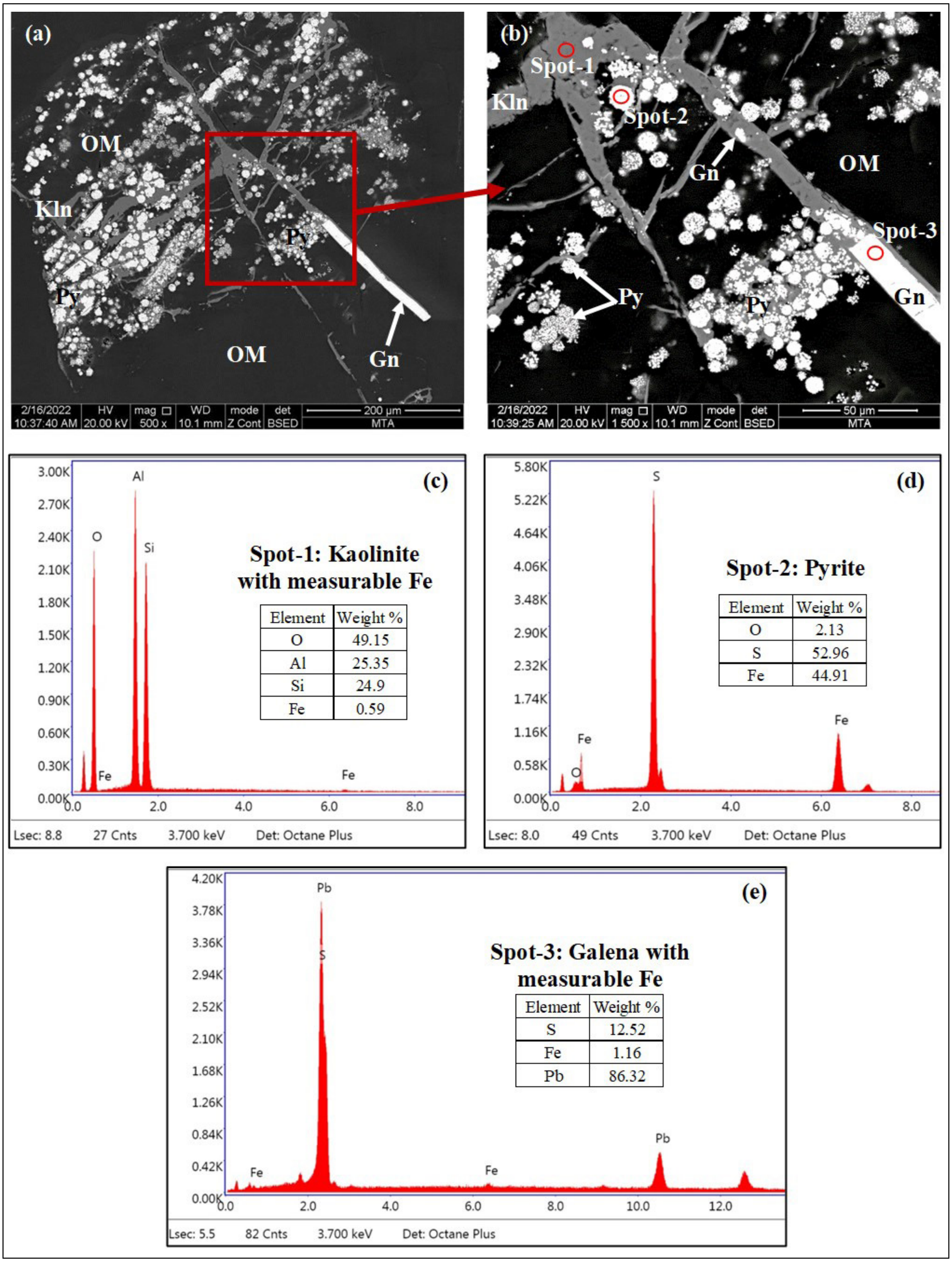

Figure 13- a), b) SEM-BSE image of cleat/fracture kaolinite (Kln) and galena (Gln)-infillings within organic matter (OM) and syngenetic framboidal pyrite (Py) grains within organic matter (OM), b) framboidal pyrite grain at spot-2, c) SEM-EDX spectra of kaolinite with measurable Fe at spot-1, and d) galena with measurable Fe at spot-2 image b. Image from K20H-O1.

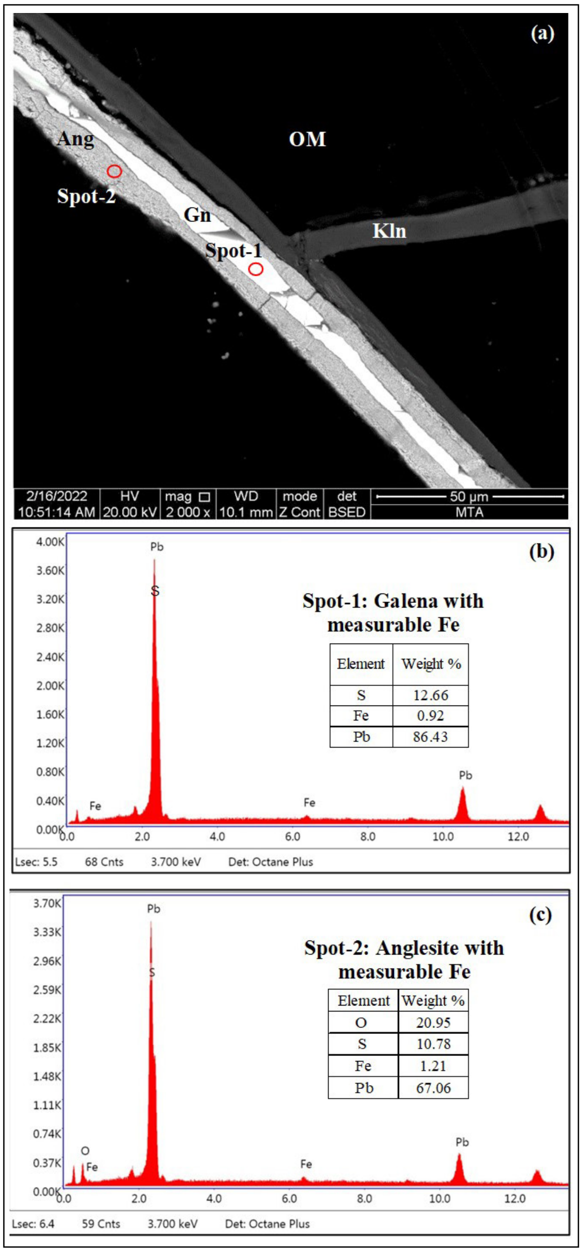

Figure 14- SEM-BSE image of cleat/fracture kaolinite (Kln), galena (Gn) and anglesite (Ang)-infillings within organic matter (OM); a) SEM-EDX spectra of galena with measurable Fe at spot-1 and b) anglesite with measurable Fe in image a. Image from K20H-O1.

in the Zonguldak Formation suggest a humid to seasonal dry climate conditions during Carboniferous (Akgün and Akyol, 1992; Opluštil et al., 2018). Under such conditions, the stability of the peat surface could be affected due to rewetting of the peat surface; in turn, peat-mires could slide, and these grains could be formed during the sliding of peat mires (Tallis, 1985; Daniels et al., 2008; Hower et al., 2021). The seasonal dry climate contains could also explain the existence of oxidized vitrinite grains in the coal clast samples from the Alacaağzı Formation. Nevertheless, the post-coalification tectonic deformation, on the other hand, could cause the formation of brecciated vitrinite grains and following the emplacement of the epigenetic mineralization, could cause elevation of the %Rr values of coal seams (Hower and Davis, 1981; Hower et al., 2001; Hower and Gayer, 2002).

This could also cause the formation of micro-cracks on vitrinite grains. Similar assumptions were also made for the Carboniferous coal seams in the studied wells and the mono- or multi-mineralic cleat/fracture infillings formed due to the penetration of hydrothermal solutions during coalification (Karayiğit et al., 2018*a*). Since brecciated vitrinite grains and carbonate mineral-infillings (e.g., pure calcite and Fe-rich dolomite/ankerite, and ankerite) are commonly observed in the Alacaağzı coal clast samples of the K20H well, the %Rr values of these coal clasts seem to be increased by tectonic deformation and following the precipitation of Ca-rich hydrothermal solutions. Furthermore, the calculated T_{peak} temperatures values of coal seams in the Alacaağzı Formation from the K20H well using Barker and Pawlewicz's (1994) formula (T_{peak}=(lnVRr%+1.19)/0.00782) range from 202 to 204 ºC (Karayiğit et al., 2018*a*); while coal clast samples from this formation in the K20H are around 220ºC, which could indicate possible hydrothermal solution penetration into embedded sediments, as like coal seams. All these imply that the erosion of paternal coal seams again took place during the late stages of peat formation and/or early coalification, and coal clasts beneath the coal seams of the Alacaağzı coal seams in the K20H well display a similar coalification pattern with coal seams in this well and penetration of hydrothermal solutions is slightly increased coalification of these clasts. In any case, the Alacaağzı coal clasts samples from the K20H well display a relatively higher coalification degree than the other studied coal clasts and coal seams in the studied wells. Although the palynological data from the coal clasts within the Alacaağzı was not reported by Akgün et al. (1997), the observed maceral composition of coal clasts in this formation is similar to the coal seams cored in the Alacaağzı Formation. This observation

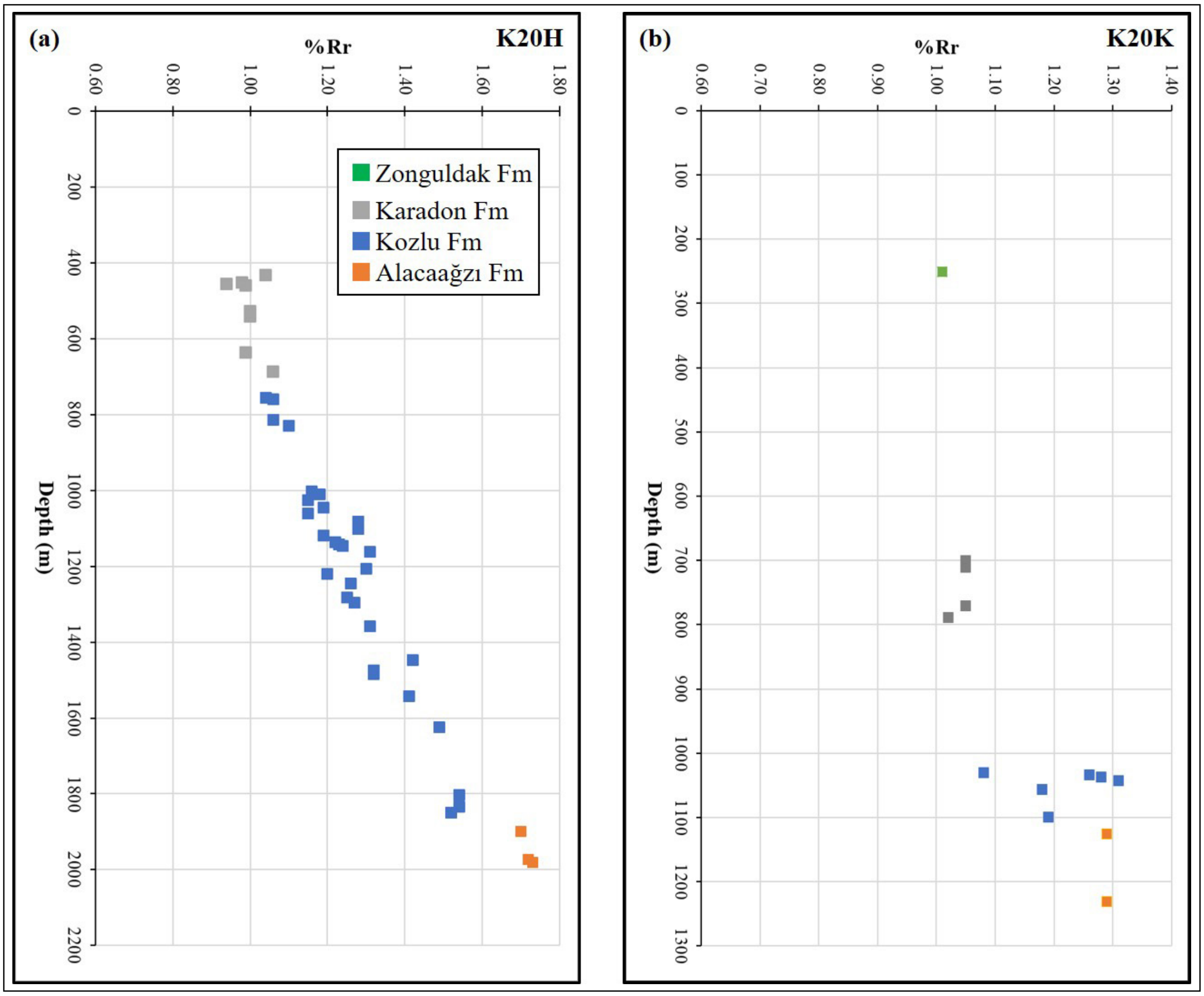

Figure 15- a) The vertical distributions of the measured $\%R_r$ from coal clasts and coal samples and calculated $\%R_r$ with depth in the K20H well and b) K20K well (%Rr data of coal samples are from Karayiğit et al., 2018*a*).

along with the close %Rr values of coal clasts (1.70-1.73%±0.03) and $\%R_{max}$ values (1.63-1.65%±0.05) of coal seams in this formation imply that the coal clast samples in the Alacaağzı Formation could be originated from coal seams from this formation.

The %Rr values (1.08-1.31% for K20H and 1.04-1.52% for K20K) of coal clast samples from the Kozlu Formation in both wells again display differences to each other (Table 2 and Figure 15), and the %Rr values of K20H samples are increased towards the

Table 4- The range of random reflectance (%Rr) values of coal clast samples and coal seams in the studied wells, and ranges of measured Rmax values of coal seams in the studied wells (a: from Karayiğit et al., 2018*a*) (Abbreviations: Stdv: standard deviation).

Wells	Formation	%Rr±Stdv of coal clast	%Rr ±Stdv of coal seam[a]	%Rmax ±Stdv of coal seam[a]
K20K	Zonguldak	1.01±0.02	-	-
	Karadon	1.02-1.05±0.02	0.78-1.01±0.04	0.82-1.10±0.03
	Kozlu	1.08-1.31±0.03	0.99-1.08±0.05	1.04-1.13±0.03
	Alacaağzı	1.29±0.03	1.18-1.28±0.07	1.22-1.35±0.03
K20H	Karadon	0.94-1.06±0.02	0.87±0.04	0.92±0.04
	Kozlu	1.04-1.52±0.03	0.97-1.46±0.06	1.00-1.57±0.07
	Alacaağzı	1.70-1.73±0.03	1.48-1.52±0.11	1.63-1.65±0.05

lower parts of the formation (Figure 15). In turn, the rank of clast samples of the Kozlu Formation in this well varies from bituminous B (medium-rank B) rank to bituminous A (medium-rank A) rank according to ISO 11750 (2005). The %Rr values of coal clasts of the Kozlu Formation in the K20K well imply a bituminous B (medium-rank B) rank. The %Rr values of the coal clast samples from this formation in both wells are relatively lower than the %Rr values of the coal seams of the formation (Table 4 and Figure 15b). Considering the presence of brecciated vitrinite and carbonate mineral-infillings, as in the Alacaağzı Formation, the relatively high %Rr values could be related to tectonic deformation and/or the influence of hydrothermal solutions. Nevertheless, the %Rr values of coal clast samples are generally within the ranges of the standard deviation of %Rr values (0.99-1.08%±0.05 for K20K and 0.97-1.46%±0.06 for K20H) of coal seams in the Kozlu Formation, and the %R_{max} values of these seams are close to the samples (Table 4). Additionally, the calculated T_{peak} values from the coal clast are between 157 and 207ºC, which is almost within the range of T_{peak} values (148-201ºC) of coal seams in Kozlu Formation in both wells (Karayiğit et al., 2018*a*). Therefore, the impact of tectonic deformation and/or hydrothermal solutions was limited to coal clasts, and the coal clasts in this formation again seem to be transported a short distance from the parental coal seams after late peat stage and/or early coalification of these seams. The existence of micro-cracks and –fissures-bearing vitrinite grains and weathered liptinite macerals (Figure 5) in the samples of the Kozlu Formation could explain relatively higher %Rr values than the coal seams in this formation. Such oxidised macerals in coal seams and coal clasts could generally develop due to surface exposure of coal-bearing sequences and/or oxidisation of coal clasts during transportation (Gayer et al., 1996; Daněk et al., 2002; Pešek and Sýkorová, 2006; Kus et al., 2017). The palynological data for the coal clast samples from the Kozlu Formation, like the coal clast samples from the Alacaağzı Formation, was not reported from the studied wells by Akgün et al. (1997); however, the observed maceral composition and close %Rr values of coal clasts and coal seams and the %R_{max} values (1.04-1.13%for K20K and 1.00-1.57% for K20H) of coal seams in this formation could imply that coal clasts presumably originated from coal seams in the Kozlu Formation.

The rank of coal clasts from the Karadon Formation in both wells is bituminous B (medium-rank B) according to ISO classification. The %Rr values (1.02-1.05%±0.02) of coal clasts samples in the K20K well are within the ranges of the %Rr values (0.78-1.01±0.04) of coal seams in this formation (Tables 2 and 4), and the %R_{max} values (0.82-1.10%) of this seam are similar to the %Rr values of coal clasts (Table 4 and Figure 15). Although one coal seam was cored in the K20H well, %Rr values (0.94-1.06%±0.02) of coal clasts are relatively higher than the %Rr values of this seam, and the %R_{max} value (0.92%±0.04) of this seam is close to %Rr values (Table 4). This difference again could be related to oxidation during transportation since micro-cracks and –fissures-bearing vitrinite grains are also observed in these samples. Furthermore, again calculated T_{peak} values (144-160ºC) of coal clasts in this formation are close to the ranges of values of coal seams (120-153ºC). Hence, coal clasts in the Karadon Formation, like other Carboniferous coal clasts, seem to have originated from the erosion of palaeomire during peat accumulation. The reported palynological data from the coal clasts from the 708.20-m in the K20K well and the coal clasts samples are approximately obtained equivalent depths with samples K20H/O4 and -O5 of by Akgün et al. (1997) support this assumption that these coal clasts were presumably originated from the Karadon Formation coal seams. Considering the Carboniferous formations (Alacaağzı, Kozlu, and Karadon) in the studied wells were deposited under fluvial conditions and the roof rocks of coal seams in these formations are generally coal clasts-bearing sandstone and/or conglomerate layers, the examined Carboniferous samples clearly originated from Carboniferous coal seams, and these seams seem to have been eroded by mainly following fluvial conditions after the peat-formation and, to a lesser extent, sliding in peat-mires during the Carboniferous. The generated 1-D model using %Rr values from the studied wells by Karayiğit et al. (2018*a*) also suggests erosional events during the Carboniferous. These also indicate that the Carboniferous coal clasts and parental coal seams generally experienced similar coalification patterns, and oxidation during transportation seems to cause relatively higher %Rr values of Carboniferous coal clast samples, which also resulted in relatively high calculated T_{peak} values of coal clasts.

The measured %Rr value (1.01%±0.02) of the coal clast sample from the Early Aptian İnciğez clastics suggests a bituminous coal rank for this clast according to ISO 11760 (2005) classification. Of note, Mann et al. (1995) and Yalçın (1995) reported that the %Rr values of Early Cretaceous sediments in the K20H research well in the Kozlu coalfield is between 0.61-0.68%. These values are lower than the investigated coal clast sample from the Zonguldak Formation in the K20K well, and %Rr value of this sample is quite similar to clast samples and coal seams from the Carboniferous formations (Table 4 and Figure 15b). Furthermore, the calculated T_{peak} value of this sample is 153ºC, while using the reported %Rr values of Early Aptian İnciğez clastics are between 89-130ºC. This difference could suggest that Early Aptian İnciğez clastics in the K20K were either affected by Cretaceous dykes in the basin or that this coal clast originated from the Carboniferous coal seams. The former case seems to be not possible due to the lack of thermally affected coal seams in both wells; nevertheless, this sample is mainly composed of telinite and collotelinite, and cleat/fracture carbonate mineral-infillings between the brecciated vitrinite grains were observed. These brecciated grains also contain micro-cracks and –fissures in this sample (Figures 3e-f). The existence of such brecciated vitrinite grains in the sample could suggest that these fragments either deformed during the coalification of parental coal seams or coal clast embedding sediments also experienced the same tectonic deformation as the encasing coal seams (Kožušníková et al., 1999; Hower et al., 2001; Xie et al., 2019). Furthermore, similar brecciated coal clasts within carbonate minerals-infillings were also reported within the Carboniferous marine carbonates in the western Kentucky coalfields (Valentim et al., 2013; 2020; Hower et al., 2020). Even though the coal metamorphism in the mentioned coalfield is quite more complex than the Kozlu coalfield, the %Rr values of brecciated clasts in the western Kentucky coalfields are high and are of anthracite-rank in comparison with Late Carboniferous seams due to high-temperature thermal-fluid metamorphism. For such metamorphism, the investigated coal clast sample from the Early Aptian İnciğez clastics should contain relict liptinite macerals and natural coke structures; however, none of these were observed in the studied Early Aptian coal clast sample. Additionally, cleat/fracture carbonate-infillings in the sample are more simply related to the precipitation of Ca-rich intra-formation solutions during diagenesis rather than the precipitation of hydrothermal solutions since the Zonguldak Formation is mainly composed of marine carbonates. Hence, this sample is more likely to be derived from the Carboniferous coal seams in the Kozlu coalfield, which was presumably eroded after the coalification of coal seams in Karadon or Kozlu formations and/or due to uplift during the Early Cretaceous, instead of hydrothermal alteration of Early Aptian coal clasts and/or xylite fragment.

6. Results

The petrographical and SEM investigations of coal clast samples from the Carboniferous and Early Aptian formations in the K20H and K20K wells imply that the majority of identified minerals in the coal clasts mainly originated from the parental coal seams, while cleat/fracture and cell lumen mineral infillings were mainly formed during mainly early coalification of parental coal seams and diagenesis of embedded sediments. Nevertheless, the relatively high %Rr values of the investigated Carboniferous coal samples in comparison with the cored coal seams in both wells are generally related to the oxidation of coal clasts during transportation since surface oxidation derived micro-cracks and –fissures are commonly observed in these samples. Furthermore, this oxidation process seems to be more severe for the coal clast samples from the Kozlu Formation, where weathered sporinite macerals are commonly identified. Despite the presence of deformed and brecciated vitrinite grains and cleat/fracture carbonate-infillings within these grains, close %Rr values of coal clasts and %Rmax values of coal seams and T_{peak} values imply that the influence of post-coalification tectonic movements and penetrated hydrothermal solutions on the coalification of these clasts is limited, and clasts and their parental coal seams exhibit similar coalification patterns. Therefore, Carboniferous coal clasts seem to have originated from the coal seams in the studied formations. Furthermore, their existence within conglomerate and sandstone layers overlying coal seams also suggest that these clasts were presumably eroded during peat formation or early coalification stages of parental coal seams by fluvial systems; nevertheless, sliding in peat mire during Carboniferous might also cause coal clast formation. The brecciated vitrinite grains could also suggest that the tectonic deformation took place during post-vitrinization event, or at least a post-lignite stage event. In contrast, coal clast samples in the Early Cretaceous Zonguldak Formation display relatively higher %Rr values than reported %Rr values of this formation, and close %Rr values with Carboniferous formations imply that this coal clast was presumably derived from eroded Late Carboniferous coal seams in the Zonguldak Basin after coalification and/or due to uplift during the Cretaceous. The cleat/fracture carbonate mineral-infillings between brecciated vitrinite grains in this sample might have developed from the precipitation of Ca-rich solutions during the diagenesis of this formation or more possibly formed during the coalification of the parental coal seam due to the presence of similar multi-mineralic cleat/ fracture infillings in the coal seams in the studied wells. Overall, all the studied coal clast samples originated from the Carboniferous coal seams in the Kozlu coalfield, and display generally similar features to Carboniferous coal clasts from central Europe and South Wales.

Acknowledgements

A part of this study is supported by the Turkish Scientific and Technological Research Council of Turkey (TÜBİTAK) under the project YDABCAG-70. The authors would like to thank Prof. Dr. J. HOWER (University of Kentucky) his suggestions during the manuscript preparations.

References

Ağralı, B. 1963. Etude des microspores du Namurien a Tarlaağzı (Amasra, Turquie). Annales de la Société Géologique du Nord t83, 145-159 (in French).

Ağralı, B. 1970. Étude des Microspores du basin Carbonifère d'Amasra. Bulletin of the Mineral Research and Exploration 75, 28-68 (in French with Turkish abstract).

Akgün, F., Akyol, E. 1992. Palynology and paleoecology of the coals in the Amasra-Bartın Carboniferous Basin Turkish Journal of Earth Sciences 1, 49-56 (in Turkish with English abstract).

Akgün, F., Uzun, N., Akyol, E. 1997. Palynology. Yalçın, M. N. (Ed.). A multidisciplinary approach on Kozlu K20/H and K20/K wells. TÜBİTAK YDABÇAG-70 Project Report, Ankara (in Turkish) (unpublished).

Akyol, E. 1972. Etudes palynologiques des veines du Namurien et du Westphalien A, recoupees par les ailes sud et est d'une galerie de cote -50a Asma, Üzülmez-Zonguldak. Bulletin of the Mineral Research and Exploration 83, 50-104 (in French with Turkish abstract).

American Society for Testing and Materials (ASTM) D2797/D2797M. 2011. Standard practice for preparing coal samples for microscopical analysis by reflected light. ASTM International, 5. Barker, C. E., Pawlewicz, M. J. 1994. Calculation of vitrinite reflectance from thermal histories and peak temperatures. A comparison of methods. Mukhopadhyay, P. K., Dow W. G. (Ed.). Vitrinite Reflectance as a Maturity Parameter: Applications and Limitations, ACS Symposium Series 570, Chicago, 216-229.

Barker, C. E., Pawlewicz, M. J. 1994. Calculation of vitrinite reflectance from thermal histories and peak temperatures. A comparison of methods. Mukhopadhyay, P. K., Dow, W. G. (Eds.). Vitrinite Reflectance as a Maturity Parameter: Applications and Limitations. ACS Symposium Series volume 570. ACS Publication, Washington, 216-229.

Bicca, M. M., Kalkreuth, W., da Silva, T. F., de Oliveira, C. H. E., Genezini, F. A. 2020. Thermal and depositional history of Early-Permian Rio Bonito Formation of southern Paraná Basin-Brazil. International Journal of Coal Geology 228, 103554.

Burger, K., Bandelow, F. K., Bieg, G. 2000. Pyroclastic kaolin coal–tonsteins of the Upper Carboniferous of Zonguldak and Amasra, Turkey. International Journal of Coal Geology 45, 39-53.

Cleal, C. J., Van Waveren, I. M. 2012. A reappraisal of the Carboniferous macrofloras of the Zonguldak-Amasra. Coal Basin, north-western Turkey. Geologia Croatica 65, 283-297.

Cleal, C. J., Stolle, E., Van Waveren, I. M., King, S., Didari, V. 2017. Carboniferous plant fossils from northern Turkey in the Jongmans Collection, Naturalis, Leiden. Paleontological Journal 51, 770-777.

Cleal, C. J., Stolle, E., Van Waveren, I. M., King, S., Didari, V. 2018. Macrofloral biostratigraphy of the upper Bashkirian Kozlu Formation, Zonguldak coalfield, north Turkey. Nurgaloev, D., Barclay, M., Nikolaeva, S., Silantiev, V., Zharinova, V., Vasilyeva O. (Ed.). Advances in Devonian, Carboniferous and Permian Research: Stratigraphy, Environments, Climate and Resources. Filodiritto, Bologna, 82-90.

Dai, S., Bechtel, A, Eble, C. F., Flores, R. M., French, D., Graham, I. T., Hood, M. M., Hower, J. C., Korasidis, V. A., Moore, T. A., Püttmann, W., Wei, Q. 2020*a*. Recognition of peat depositional environments in coal: A review. International Journal of Coal Geology 219, 103383.

Daněk, V., Pešek, J., Valterová, P. 2002. Coal clasts in the Bolsovian (Westphalian C) sequence of the Kladno-Rakovník continental basin (Czech Republic): implication of the timing of maturation. Polish Geological Institute Special Paper 7, 63-78.

Daniels, S. M., Agnew, C. T., Allott, T. E. H., Evans, M. G. 2008. Water table variability and runoff generation in an eroded peatland, South Pennines, UK. Journal of Hydrology 361, 214-226.

Dawson, G. K. W., Golding, S. D., Esterle, J. S., Massarotto, P. 2012. Occurrence of minerals within fractures and matrix of selected Bowen and Ruhr Basin coals. International Journal of Coal Geology 94, 150-166.

Dill, H. G., Kus, J., Kaufhold, S., Rammlmair, D., Techmer, A. 2017. Oligo-Miocene coal in a microtidal environment reworked under Quaternary periglacial conditions (Western Falkland Islands/ Isla Gran Malvina) coal formation and natural sand processing. International Journal of Coal Geology 174, 8-22.

Dill, H. G., Kus, J., Andrei, B., Sorin-Ionut, B., Stephan, K., Borrego, A. G. 2021. Organic debris and allochthonous coal in Quaternary landforms within a periglacial setting (Longyearbyen Mining District, Norway) - A multi-disciplinary study (coal geology-geomorphology-sedimentology). International Journal of Coal Geology 233, 103625.

Gayer, R. A., Pešek, J., Sýkorová, I., Valterová, P. 1996. Coal clasts in the upper Westphalian sequence of the South Wales coal basin: Implications for the timing of maturation and fracture permeability. Geological Society Special Publication 109, 103-120.

Geršlová, E., Goldbach, M., Geršl, M., Skupien, P. 2016. Heat flow evolution, subsidence and erosion in Upper Silesian Coal Basin, Czech Republic. International Journal of Coal Geology 154-155, 30-42.

Gürdal, G., Yalçın, M. N. 2000. Gas adsorption capacity of Carboniferous coals in the Zonguldak Basin (NW Turkey) and its controlling factors. Fuel 79, 1913-1924.

Gürdal, G., Yalçın, M. N. 2001. Pore volume and surface area of the carboniferous coal from the Zonguldak Basin (NW Turkey) and their variations with rank and maceral composition. International Journal of Coal Geology 48, 133-144.

Gürdal, G., Mann, U., Yalçın, M. N. 2004. Comparison of adsorption related properties of Zonguldak Basin coals (NW Turkey) obtained at two different adsorption temperatures of carbon dioxide. Energy Source 26, 1301-1312.

Hower, J. C., Davis, A. 1981. Vitrinite reflectance anisotropy as a tectonic fabric element. Geology 9, 165-168.

Hower, J. C., Gayer, R. A. 2002. Mechanisms of coal metamorphism: case studies from Paleozoic coalfields. International Journal of Coal Geology 50, 215-245.

Hower, J. C., Williams, D. A., Eble, C. F., Sakulpitakphon, T., Moecher, D. P. 2001. Brecciated and mineralized coals in Union County, Western Kentucky coal field. International Journal of Coal Geology 47, 223-234.

Hower, J. C., O'Keefe, J. M. K., Valentim, B., Guedes, A. 2021. Contrasts in maceral textures in progressive metamorphism versus near-surface hydrothermal metamorphism. International Journal of Coal Geology 246, 103840.

International Committee for Coal Petrology (ICCP). 1998. The new vitrinite classification (ICCP System 1994). Fuel 77, 349-358.

International Committee for Coal Petrology (ICCP). 2001. New inertinite classification (ICCP System 1994). Fuel 80, 459-471.

International Organisation for Standardization (ISO) 11760. 2005. Classification of coals. International Organization for Standardization, 9.

International Organization for Standardization (ISO) 7404–5. 2009. Methods for the Petrographic Analysis of Coal—Part 5: Method of determining microscopically the reflectance of vitrinite. International Organization for Standardization, 4.

Izart, A., Barbarand, J., Michels, R., Privalov, V.A. 2016. Modelling of the thermal history of the Carboniferous Lorraine Coal Basin: Consequences for coal bed methane. International Journal of Coal Geology 168, 253-274.

Karayiğit, A. I. 1992. Linear relations among vitrinite reflections of coals in Zonguldak and Amasra basins. Turkish Journal of Earth Sciences 1, 43-48 (in Turkish with English abstract).

Karayiğit, A. I., Gayer, R. A., Demirel, I. H. 1998. Coal rank and petrography of Upper Carboniferous seams in the Amasra Coalfield Turkey. International Journal of Coal Geology 36, 277-294.

Karayiğit, A. I., Littke, R., Querol, X., Jones, T., Oskay, R. G., Christanis, K. 2017. The Miocene coal seams in the Soma Basin (W. Turkey): Insights from coal petrography, mineralogy and geochemistry. International Journal of Coal Geology 173, 110-128.

Karayiğit, A. I., Mastalerz, M., Oskay, R. G., Gayer, R. A. 2018*a*. Coal petrography, mineralogy, elemental compositions and palaeoenvironmental interpretation of Late Carboniferous coal seams in three wells from the Kozlu coalfield (Zonguldak Basin, NW Turkey). International Journal of Coal Geology 187, 54-70.

Karayiğit, A. I., Mastalerz, M., Oskay, R. G., Buzkan, İ. 2018*b*. Bituminous coal seams from underground mines in the Zonguldak Basin (NW Turkey): Insights from mineralogy, coal petrography, rock-eval pyrolysis, and meso-and microporosity. International Journal of Coal Geology 199, 91-112.

Karayiğit, A. I., Oskay, R. G., Bulut, Y., Mastalerz, M. 2020. Meso- and microporosity characteristics of Miocene lignite and subbituminous coals in the Kınık coalfield (Soma Basin, W. Turkey). International Journal of Coal Geology 232, 103624.

Kerey, I. E. 1985. Facies and Tectonic Setting of the Upper Carboniferous Rocks of NW Turkey. Robertson, A. H. F., Dixon J. E. (Ed.). The Geological Evolution of the Eastern Mediterranean. Geological Society of London Special Publication 17, Geological Society of London, 123-128.

Küskü, O., Canca, N., Hoşgörmez, H., İnan, S., Yalçın, M. N. 1997. Geology. In: Yalçın, M. N. (Ed.). A multidisciplinary approach on Kozlu-K20/H and K20/K research wells. TÜBİTAK YDABÇAG-70 Project Report, Ankara (in Turkish) (unpublished).

Kožušníková, A., Martinec, P., Pešek, J., Valterová, P. 1999. Coal clasts in the Carboniferous sediments of the Upper Silesian basin. Bulletin of Geosciences 74, 109-114.

Kus, J., Misz-Kennan, M., International Committee for Coal and Organic Petrology. 2017. Coal weathering and laboratory (artificial) coal oxidation. International Journal of Coal Geology 171, 12-36.

Liu, J., Dai, S., Song, H., Nechaev, V. P., French, D., Spiro, B. F., Graham, I. T., Hower, J. C., Shao, L., Zhao, J. 2021. Geological factors controlling variations in the mineralogical and elemental compositions of Late Permian coals from the Zhijin-Nayong Coalfield, western Guizhou, China. International Journal of Coal Geology 247, 103855.

Littke, R., Horsfield, B., Leythauser, D. 1989. Hydrocarbon distribution in coals and in dispersed organic matter of different maceral compositions and maturities. Geologische Rundschau 78, 391-410.

Mann, U., Hertle, M., Horsfield, B., Radke, M., Schenk, H. J., Yalçın, M. N. 1995. Petrographical, organic-geochemical and petrophysical characterization of Upper Carboniferous coals from well K20/H, Zonguldak Basin. Yalçın, M. N., Gürdal, G. (Ed.). Zonguldak Basin Research Wells-1. Special Publication of TÜBİTAK Marmara Research Centre, Kocaeli, 133-166.

Martínek, K., Pešek, J., Opluštil, S. 2017. Significant hiatuses in the terrestrial Late Variscan Central and Western Bohemian basins (Late Pennsylvanian-Early Cisuralian) and their possible tectonic and climatic links. Geologica Carpathica 68, 269-281.

Misz-Kennan, M., Fabiańska, M., Ciesielczuk J., Filipiak, P., Jura, D. 2019. Organic geochemistry and petrography of coal clasts deposited in Pennsylvanian sandstones (upper Silesian coal basin, Poland). 29th International Meeting on Organic Geochemistry (IMOG), 1–6 September 2019, Gothenburg, 1-2.

Oktay, F. A. 1995. Sedimentological and petrographical properties of Carboniferous sequence drilled by K20/G well. Yalçın, M. N., Gürdal, G. (Ed.). Zonguldak Basin Research Wells-I. TÜBİTAK-MAM Special Publications, Kocaeli, 73-98 (in Turkish with English abstract).

Okay, A. I., Nikishin, A. M. 2015. Tectonic evolution of the southern margin of Laurasia in the Black Sea region. International Geology Reviews 57, 1051-1076.

Okay, A. I., Şengör, A. M. C., Görür, N. 1994. Kinematic history of the opening of the Black Sea and its effect on the surrounding regions. Geology 22, 267-270.

Opluštil, S., Lojka, R., Pšenička, J., Yilmaz, Ç., Yılmaz, M. 2018. Sedimentology and stratigraphy of the Amasra coalfield (Pennsylvanian), NW Turkey – new insight from a 1 km thick section. International Journal of Coal Geology 195, 317-346.

Paszkowski, M., Jachowicz, M., Michalik, M., Teller, L., Uchman, A., Urbanek, Z. 1995. Composition, age and provenance of gravel-sized clasts from the Upper Carboniferous of the Upper Silesia Coal Basin (Poland). Studia Geologica Polonica 108, 45-127.

Petersen, H. I., Bojesen-Koefoed, J. A., Nytoft, H. P., Surlyk, F., Therkelsen, J., Vosgerau, H. 1998. Relative sea-level changes recorded by paralic liptinite-enriched coal facies cycles, Middle Jurassic Muslingebjerg Formation, Hochstetter Forland, Northeast Greenland. International Journal of Coal Geology 36, 1-30.

Pešek, J., Sýkorová, I. 2006. A review of the timing of coalification in the light of coal seam erosion, clastic dykes and coal clasts. International Journal of Coal Geology 66, 13-34.

Permana, A. K., Ward, C.R., Li, Z., Gurba, L. W. 2013. Distribution and origin of minerals in high-rank coals of the South Walker Creek area, Bowen Basin, Australia. International Journal of Coal Geology 116–117, 185-207.

Pickel, W., Kus, J., Flores, D., Kalaitzidis, S., Christanis, K., Cardott, B. J., Misz-Kennan, M., Rodrigues, S., Hentschel, A., Hamor-Vido, M., Crosdale, P., Wagner, N., ICCP. 2017. Classification of liptinite-ICCP System 1994. International Journal of Coal Geology 169, 40-61.

Rodrigues, S., Esterle, J., Ward, V., Glasser, L., Maquissene, T., Etchart, E. 2020. Flow structures and mineralisation in thermally altered coal from the Moatize Basin, Mozambique. International Journal of Coal Geology 228, 103551.

Suchý, V., Filip, J., Sýkorová, I., Pešek, J., Kořínková, D. 2019. Palaeo-thermal and coalification history of Permo-Carboniferous sedimentary basins of central and Western Bohemia, Czech Republic: first insights from apatite fission track analysis and vitrinite reflectance modelling. Bulletin of Geosciences 94, 201-219.

Tallis, J. H. 1985. Mass movement and erosion of a southern Pennine blanket peat. Journal of Ecology 73, 283-315.

Tüysüz, O., Melinte-Dobrinescu, M. C., Yılmaz, İ. Ö., Kirici, S., Švabenická, L., Skupien, P. 2016. The Kapanboğazı formation: A key unit for understanding Late Cretaceous evolution of the Pontides, N Turkey. Palaeogeography, Palaeoclimatology, Palaeoecology 441, 565-581.

Xie, P., Hower, J. C., Liu, X. 2019. Petrographic characteristics of the brecciated coals from Panxian county, Guizhou, southwestern China. Fuel 243, 1-9.

Valentim, B., Hower, J. C., O'Keefe, J. M. K., Rodrigues, S., Riberio, J., Guedes, A. 2013. Notes on the origin of altered macerals in the Ragged Edge of the Pennsylvanian (Asturian) Herrin coalbed, Western Kentucky. International Journal of Coal Geology 115, 24-40.

Valentim, B., Couto, H., French, D., Golding, S. D., Guimarães, F., Guedes, A., O'Keefe, J. M. K., Raymond, A. L., Santos, C., Valian, A., Ward, C. R., Hower, J. C. 2020. Could hot fluids be the cause of natural pyrolysis at the ragged edge of Herrin coal, Millport 7 ½' quadrangle, Hopkins County, Kentucky. International Journal of Coal Geology 231, 103603.

Yalçın, M. N. 1995. Contribution of the Kozlu-K20/G well to the computer-aided modelling studies in the Zonguldak Basin. Yalçın, M. N., Gürdal, G. (Ed.). Zonguldak Basin Research Wells-I. TÜBİTAK-MAM Special Publications, Kocaeli, 173-196 (in Turkish with English abstract).

Yalçın, M. N., Inan, S., Gürdal, G., Mann, U., Schaefer, R. G. 2002. Carboniferous coals of the Zonguldak Basin (northwest Turkey): Implications for coalbed methane potential. AAPG Bulletin 86, 1305-1328.

Yang, G., Huang, W., Zhong, J., Sun, N. 2020. Occurrence, classification and formation mechanisms of the organic-rich clasts in the upper Paleozoic coal-bearing tight sandstone, northeastern margin of the Ordos Basin, China. Energies 13, 2694.

Yürüm, Y., Dilara, B., Yalçın, M. N. 2001*a*. Change of the structure of coals from the Kozlu K20 G borehole of Zonguldak Basin with burial depth 1. Chemical structure. Energy Source 23, 511-520.

Yürüm, Y., Dilara, B., Yalçın, M. N. 2001*b*. Change of the structure of coals from the KozluK20 G borehole of Zonguldak Basin with burial depth 2. Macromolecular structure. Energy Source 23, 521-527.

Zhang, T., Wang, R., Polyak, L., Xiao, W. 2019. Enhanced deposition of coal fragments at the Chukchi margin, western Arctic Ocean: Implications for deglacial drainage history from the Laurentide Ice Sheet. Quaternary Science Reviews 218, 281-292.

Zhao, L., Ward, C. R., French, D., Graham, I. T., Dai, S., Yang, C., Xie, P., Zhang, S. 2018. Origin of a kaolinite-NH_4-illite-pyrophyllite-chlorite assemblage in a marine-influenced anthracite and associated strata from the Jincheng Coalfield, Qinshui Basin, Northern China. International Journal of Coal Geology 185, 61-78.

Zijlstra, G. 1952. Erosion of the Namurian during the Westphalian b-c in the Zonguldak coal field (Turkey). Bulletin of Mineral Research and Exploration 42-43, 121-122.